Supporting Information

A Non-Rigid Supramolecular Host with a Cavitand Core and Four Cholate Side Arms

Beijun Cheng*,[a] Marcos D. García,[b] Yan Tian,[a] Carlos Peinador[b] Yuezhi Cui,[a] Qingqing Lu,[a] Yuexia Qin,[c] Zhaohua Hou,[c] and Angel E. Kaifer*,[d]

[a]School of Chemistry and Chemical Engineering, Qilu University of Technology (Shandong Academy of Sciences), Jinan, 250353, China, [b]Departamento de Química and Centro Interdisciplinar de Química e Bioloxía (CICA). Facultad de Ciencias, Universidade da Coruña, 15071 A Coruña, Spain, [c]School of Food Science and Engineering, Qilu University of Technology (Shandong Academy of Sciences), Jinan, 250353, China [d]Department of Chemistry, University of Miami, Coral Gables, FL 33124, U.S.A.

akaifer@miami.edu

bchengsd@163.com

Table of Contents

1. Synthetic Procedures and Characterization Data:

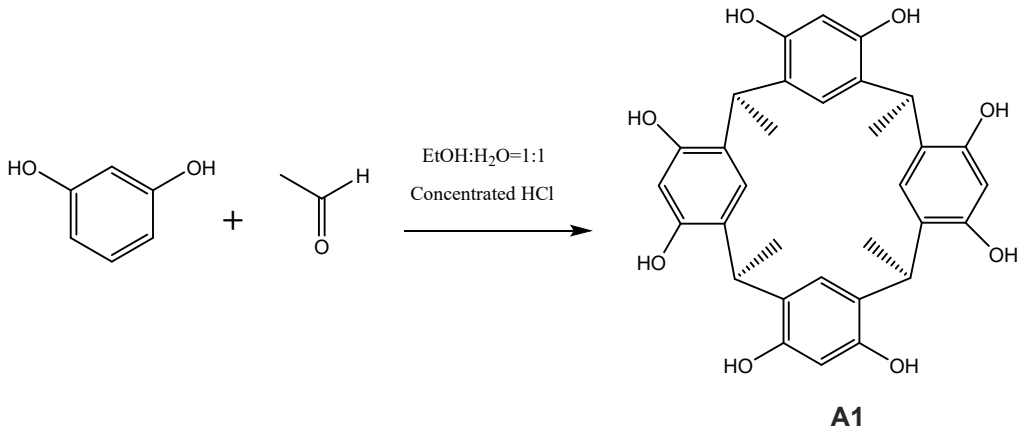

A1

Scheme S1. Synthesis of Compound **A1**

2,8,14,20-Tetramethylresorc[4]arene (A1)[1] **:** Resorcinal (33.03 g, 0.3 mol) was dissolved in 60 mL of ethanol, 60 mL of water and 60 mL of aqueous HCl (36%-38%).The solution was cooled to around 0 °C by immersing in an ice bath, followed by the slow addition of CH_3CHO (8.81 g, 0.2 mol). Then the solution mixture was stirred in an oil bath at 80°C for 20 h. The yellow precipitate was filtered and washed with cold 1:1 ethanol:water and dried under vacuum to give 28.3 g (69%) of **A1** as a pale yellow solid**.** ^{1}H NMR (400 MHz, $(CD_3)_2SO$): *δ* 8.53 (s, 8H), 6.77 (s, 4H), 6.14 (s, 4H), 4.46 (q, 4H), 1.31 (d, 12H).

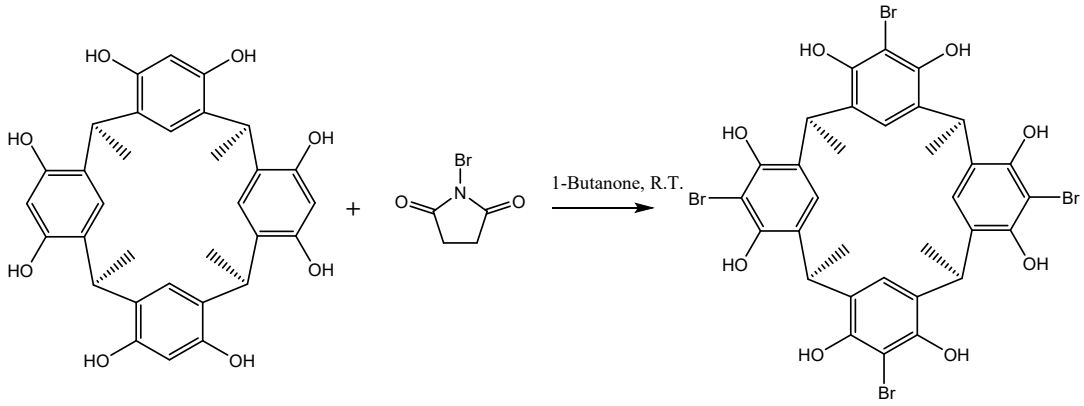

A1 **A2**

Scheme S2. Synthesis of Compound **A2**

5,11,17,23-Tetrabromo-2,8,14,20-tetramethylpentacyclo[19.3.1.1^{3,7}.1^{9,13}.1^{15,19}]octacosa-1(25),3,5,7(28),9,11,13(27),15,17,19(26),21,23-dodecaene-4,6,10,12,16,18,22,24-octol(A2)[1] **: A1**(1.5 g, 2.75 mmol) was dissolved in 35 mL of 2-butanone, followed by the slow addition of 3.9 g (22.0 mmol) of *N*-bromosuccinimide (recrystallized from boiling water). The reaction mixture was stirred at R.T. for 5 h and the precipitate was filtered and washed with hot CH_2Cl_2 to give 1.85 g (78%) of **A2** as a white solid. ^{1}H NMR (400 MHz, $(CD_3)_2SO$): *δ* 8.38 (s, 8H), 6.80 (s, 4H), 4.62 (q, 4H), 1.40 (d, 12H).

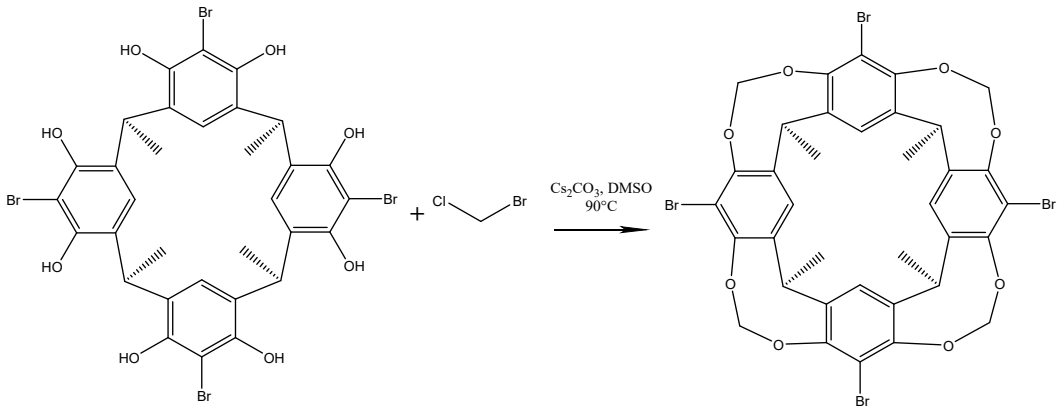

A2 **A3**

Scheme S3. Synthesis of Compound **A3**

7,11,15,28-tetrabromo-1,21,23,25-tetramethyl-2,20:3,19-dimetheno-1*H*,21*H*,23*H*,25*H*-bis[1,3]dioxocino[5,4-*i*:5′,4′-*i*′]benzo[1,2-*d*:5,4-*d*′]bis[1,3]benzodioxocin (A3)[2] **: A2**(2.39 g, 2.78 mmol) and Cs_2CO_3(7.17 g, 22.0 mmol), CH_2BrCl (7.17 mL, 110.34 mmol) were added to dry DMSO (60 mL) in a seal vessel (Synthware™ pressure vessel). The mixture was stirred in an oil bath at 80 °C for 3 h. (Caution: Changes in the reaction conditions may result in much larger internal pressures.) After cooling to R.T., the mixture was poured in to 200 mL of 2% aqueous HCl. The precipitate was filterred, washed with H_2O and dried under vacuum. The product was alreay very pure. To meet the strict reaction condition of next step, it was purifed by column chromatography over silica gel using CH_2Cl_2 (100%) as the eluent to give 2.23 g (91%) of **A3** as a white solid. ^{1}H NMR (400 MHz, $CDCl_3$): *δ* 7.17 (s, 4H), 5.98 (d, 4H), 5.09 (q, 4H), 4.42(d, 4H), 1.77(d, 12H).

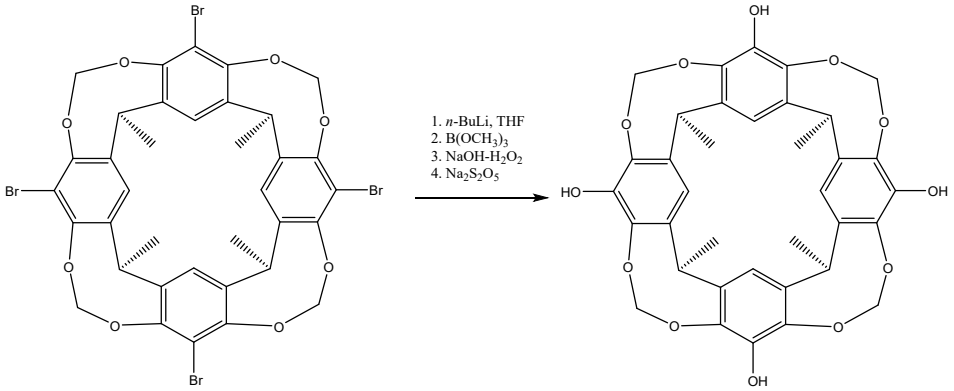

A3 **A4**

Scheme S4. Synthesis of Compound **A4**

1,21,23,25-Tetramethyl-2,20:3,19-dimetheno-1*H*,21*H*,23*H*,25*H*-bis[1,3]dioxocino[5,4-*i*:5',4'-*i*']benzo[1,2-*d*:5,4-*d*']bis[1,3]benzodioxocin-

7,11,15,28-tetrol(A4)[3,4] **: A3** (2.0 g, 2.2 mmol) was added to dry THF(150 mL). The solution was cooled to -70 °C. Under N_2, n-BuLi (44.0 mL of a 1.6 M solution in hexane, 70.4 mmol) was added. The reaction temperature was slowly increased to around -25 °C and stirred for 1 h. Then the reaction temperature was decreased to -70°C again, and $B(OMe)_3$ (9 mL, 80.7 mmol) was slowly added. Afterwards, reaction temperature was gradually increased to room temperature and the solution was stirred at R.T. for 1 h. The reaction mixture was cooled to -70°C again and 1.5 M NaOH-15%H_2O_2 (80 mL) was slowly added. The dry ice-ethanol bath was removed and the reaction mixture was stirred overnight. After being cooled to 0 °C in an ice bath, $Na_2S_2O_5$ (40 g, 210 mmol) was added. THF was removed under vacuum and white precipitate formed during the THF evaporation. The precipitate was filtered and washed with H_2O. The crude product was purified by column chromatography over silica gel by using EtOAc:hexane (3:1) to afford 0.46 g (32%) of **A4** as a white solid. ^{1}H NMR (400 MHz, $(CD_3)_2CO$): *δ* 7.87 (s, 4H), 7.12 (s, 4H), 5.82 (d, 4H), 4.89 (q, 4H), 4.40 (d, 4H), 1.75 (d, 12H).

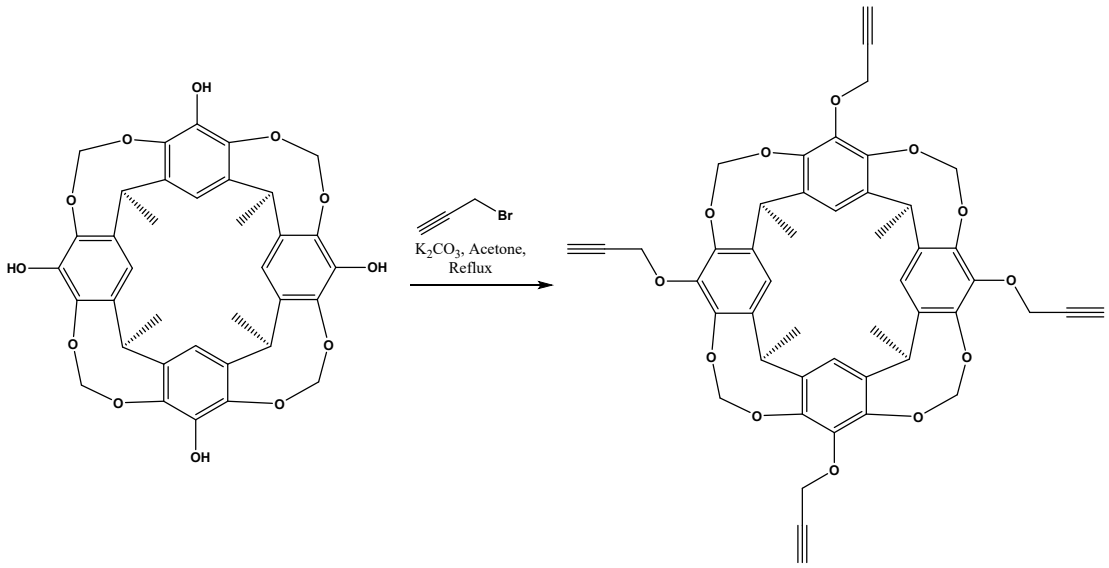

A4 **2**

Scheme S5. Synthesis of Compound **2**

1,21,23,25-tetramethyl-7,11,15,28-tetrakis(2-propyn-1-yloxy)-2,20:3,19-dimetheno-1*H*,21*H*,23*H*,25*H*-bis[1,3]dioxocino[5,4-*i*:5′,4′-*i*′]benzo[1,2-*d*:5,4-*d*′]bis[1,3]benzodioxocin (2)[5] **: A4** (150 mg, 0.228 mmol) was dissolved in 25 mL of acetone, followed by the addition of propargyl bromide (0.26 mL, 3.42 mmol) and K_2CO_3 (380 mg, 2.75 mmol). The mixture was refluxed in an oil bath for 24 h. The solvent was removed under vacuum. The crude product was redissolved in CH_2Cl_2 and filtered to remove insoluble impurity. Then the crude product was purified on a column chromatography over silica gel using CH_2Cl_2:EtOAc (1:5) as the eluent to afford 160 mg (87%) of **2** as a white solid**.** ^{1}H

NMR (400 MHz, $CDCl_3$): δ 6.95 (s, 4H), 5.91(d, 4H), 4.96 (q, 4H), 4.61(d, 8H), 4.41(d, 4H), 2.47(t, 4H), 1.74(d, 12H). $^{13}C\{^1H\}$ NMR (100 MHz, $CDCl_3$): δ 148.0, 143.3, 139.9, 114.4, 99.7, 79.5, 75.0, 60.8, 31.3, 16.0.

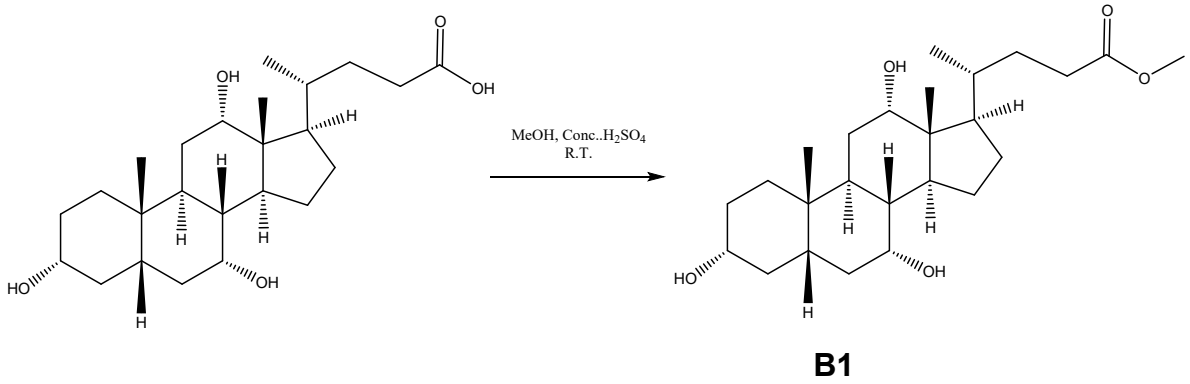

Scheme S6. Synthesis of Compound **B1**

Methyl 3α, 7α, 12α -trihydroxy-5β-cholan-24-oate (B1) [6] **:** To a solution of 3α,7α,12α-Trihydroxy-5β-cholan-24-oic acid (13 g, 31.8 mmol) in 300 mL of absolute methanol was added 0.22 mL concentrated H_2SO_4. The solution was refluxed in an oil bath for 3 h. After cooling to room temperature, the mixture was poured into 600 mL H_2O. The precipitate was filtered and washed with H_2O and dried under vacuum to give 13.3 g (99%) of **B1** as a white solid. ^1H NMR (400 MHz, CD_3OD): δ 3.94 (s, 1H), 3.79 (s, 1H), 3.64 (s, 3H), 3.40-3.33 (m, 1H), 2.42-1.06 (m, 24H), 1.01 (d, 3H), 0.91 (s, 3H), 0.71 (s, 3H).

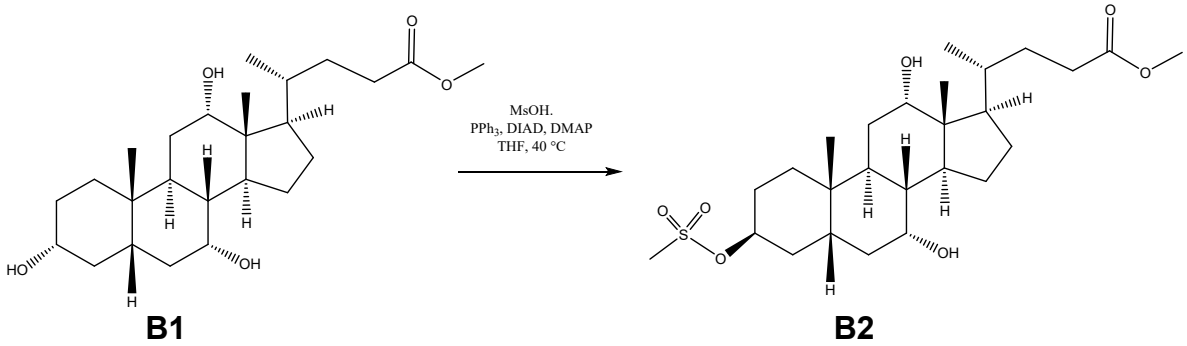

Scheme S7. Synthesis of Compound **B2**

Methyl 7α,12α-dihydroxy-3β-[(methylsulfonyl)oxy]-5β-cholan-24-oate (B2) [7,8]: **B1**(2.5 g, 5.9 mmol) and PPh_3 (3.67 g, 14.0 mmol) was dissolved in dry THF (50 mL). DMAP(1.47 g, 12 mmol) and MsOH (0.78 mL, 12 mmol) were added to the solution, followed by the slow addition of DIAD (2.76 mL, 14 mmol). The mixture was stirred in an oil bath at 40 °C for 15 h. After cooling to the R.T., the reaction mixture was filtered through a sintered funnel with Celite. The filtrate was concentrated under vacuum. The concentrate was redissolved in CH_2Cl_2, washed with diluted HCl and saturated $NaHCO_3$ solution and H_2O, dried over anhydrous $MgSO_4$, concentrated under vacuum and purified by flash

chromatography over silica gel using EtOAc:hexane (3:1) affording 1.06 g (36%) of **B2** as a white solid. ^{1}H NMR (400 MHz, $CDCl_3$): δ 4.98 (bs, 1H), 4.00 (s, 1H), 3.87 (s, 1H), 3.67 (s, 3H), 3.00 (s, 3H), 2.64-1.10 (m, 26H), 0.98 (d, 3H), 0.96 (s, 3H), 0.70 (s, 3H).

B2 **B3**

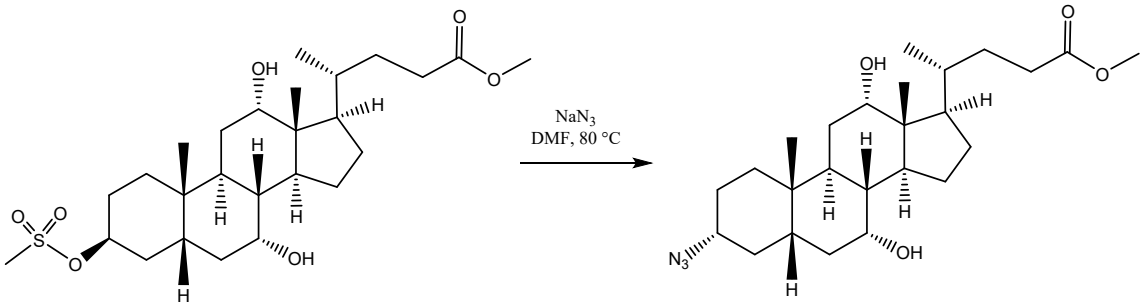

Scheme S8. Synthesis of Compound **B3**

Methyl 3α-azido-7α,12α-dihydroxy-5β-cholan-24-oate (B3)[7-9]**: B2**(0.85 g, 1.7 mmol) was dissolved in DMF (10 mL), followed by the addition of NaN_3 (0.22 g, 3.4 mmol). The solution mixture was stirred in an oil bath at 75 °C for 8 h. After cooling to R.T., the solution mixture was poured into 30 mL H_2O and was extracted with EtOAc (30 mL x 2). The organic layer was washed with H_2O and dried over anhydrous $MgSO_4$. The crude product was purified by column chromatography over silica gel using EtOAc:hexane(1:4) to give 0.52 g (68%) of **B3** as a white solid.^{1}H NMR (400 MHz, $CDCl_3$): δ 3.99 (s, 1H, H-12β), 3.87 (s, 1H), 3.67 (s, 3H), 3.19-3.13 (m, 1H), 2.99 (s, 3H), 2.42-1.09 (m, 26H), 0.99 (d, 3H), 0.91 (s, 3H), 0.69 (s, 3H).

B3 **3**

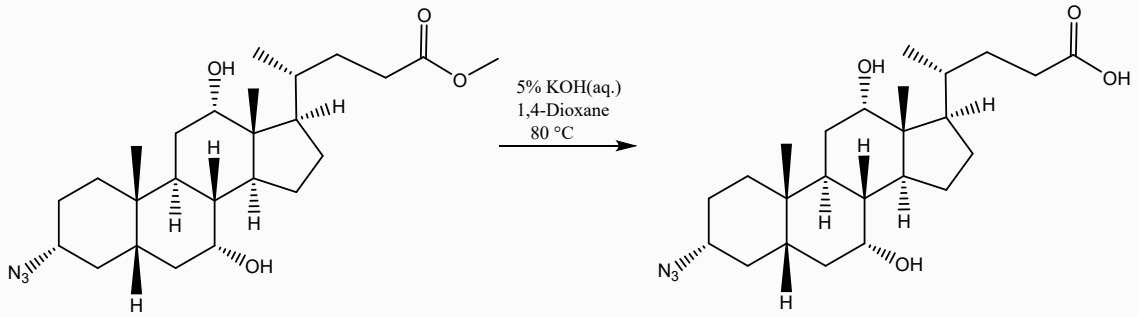

Scheme S9. Synthesis of Compound **3**

3α-Azido-7α, 12α-dihydroxy-5β-cholan-24-oic acid (3)[7]: B3 (1.0 g, 2.23 mmol) was dissolved in 1,4-dioxane (25 mL), aq. KOH (5% w/v, 25 mL). The mixture was stirred in an oil bath at 80 °C for 3 h. After cooling to R.T. the reaction mixture was acidified with dil. HCl to a pH of 5-6 and extracted with EtOAc (30 mL x 3). The organic layer was washed with H_2O and dried over anhydrous $MgSO_4$. The crude product was purified by column chromatography on silica gel using EtOAc (100%) to give 0.89 g (92%) of **3** as a white solid**.** ^{1}H NMR (400 MHz, CD_3OD): *δ* 3.95 (s, 1H), 3.80 (s, 1H), 3.20-3.12 (m, 1H), 2.44-1.07 (m, 24H), 1.02 (d, 3H), 0.93 (s, 3H), 0.71 (s, 3H). ^{13}C{^{1}H} NMR (100 MHz, $(CD_3)_2SO$): *δ* 175.0, 71.0, 66.1, 60.8, 46.1, 45.8, 41.5, 41.4, 35.0, 35.0, 35.0, 34.5, 34.3, 30.8, 30.8, 28.4, 27.3, 26.3, 26.1, 22.7, 22.5, 17.0, 12.3.

1,1'-Dimethyl-4,4'-bipyridinium diiodide (MV^{2+}): 4,4'-Bipyridine (1.6 g, 10.2 mmol) and iodomethane (1.6 mL, 25.6 mmol) were dissolved in 100mL anhydrous acetonitrile in a seal vessel (Synthware™ pressure vessel). The mixture was stirred in an oil bath at 78 °C for 6 h. (Caution: Changes in the reaction conditions may result in much larger internal pressures.) After cooling to room temperature, 100 mL of ethyl acetate was added. The precipitate was filterred and washed with EtOAc to afford 4.25 g product (94.3%) as an orange solid. ^{1}H NMR (400 MHz, D_2O): *δ* 9.03 (d, 4H), 8.50 (d, 4H), 4.46 (s, 6H).

1,1'-Butyl-4,4'-bipyridinium dibromide (BV^{2+}): 4,4'-Bipyridine (1.56 g, 10.0 mmol) and 1-bromobutane (3.14 mL, 30.0 mmol) was dissolved in 20 mL of acetonitrile. The mixture was stirred in an oil bath at 76 °C for 48 h. The precipitate was filtered and washed with diethyl ether to removed unreacted 4,4'-bipyridine to afford 3.53 g product (82%) as a yellow solid. ^{1}H NMR (400 MHz, $(CD_3)_2SO$): *δ* 9.43 (d, 4H), 8.82 (d, 4H), 4.71 (t, 4H), 1.97 (qu, 4H), 1.35 (sept, 4H), 0.94 (t, 6H).

1′-Ethyl-1-heptyl-4,4′-bipyridinium dibromide (EHV^{2+}): 4,4'-Bipyridine (4.0 g, 25.6 mmol) was dissolved in 40 mL of acetonitrile, followed by the addition of bromoethane (0.38 mL, 5.0 mmol) in a seal vessel (Synthware™ pressure vessel). (Caution: Changes in the reaction conditions may result in much larger internal pressures.) The mixture was stirred in an oil bath at 76 °C for 12 h. The solvent was removed under vacuum and the crude product was redissolved in DMF. The undissolved impurity was filterred off and the filtrate was added diethyl ether to precipitate the product out and the product was washed with diethyl ether to afford 1.13 g of 1-ethyl-4,4'-bipyridinium. 500 mg (1.89 mmol) of 1-ethyl-4,4'-bipyridinum was dissolved in 20 mL of acetonitrile, followed by the addition of 1-bromoheptane (1.5 mL, 10 mmol). The mixture was stirred in an oil bath at 70 °C for 24 h. The precipitate was filtered and washed with acetonitrile to afford 350 mg product (41.7%) as a yellow solid. ^{1}H NMR (400 MHz, $(CD_3)_2SO$): *δ* 9.45 (q, 4H), 8.84 (d, 4H), 4.74 (m, 4H), 1.98 (qu, 2H), 1.61 (t, 3H), 1.31 (m, 8H), 0.87 (t, 3H).

2. ^{1}H NMR, ^{13}C NMR and MS Spectra

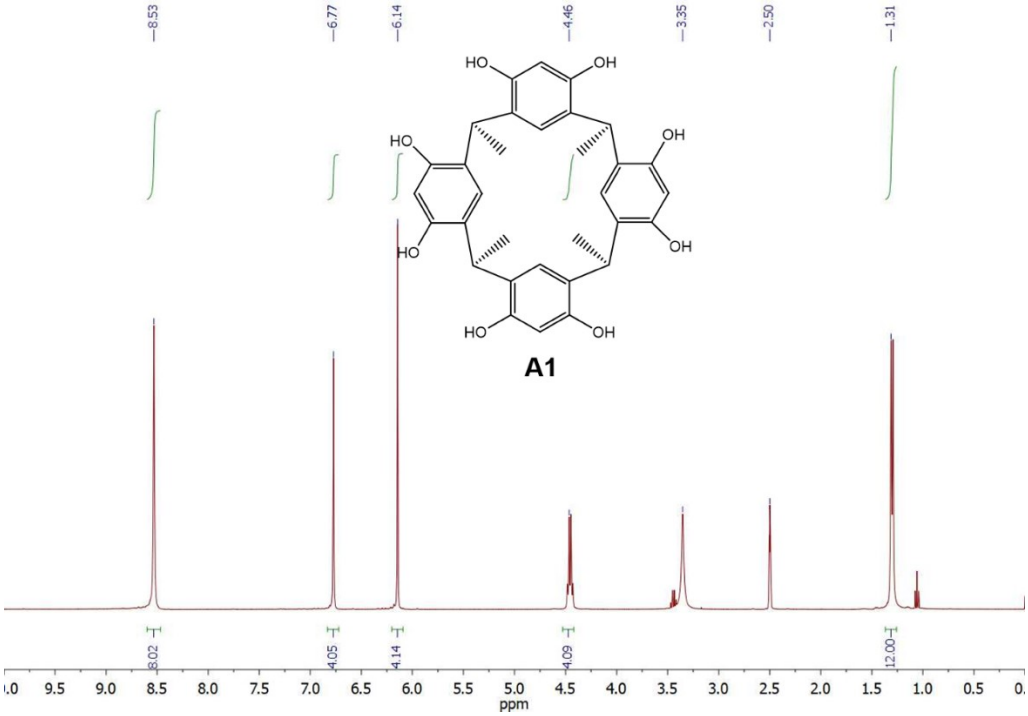

Figure S1: ^{1}H NMR Spectrum (400 MHz, $(CD_3)_2SO$) of **A1**

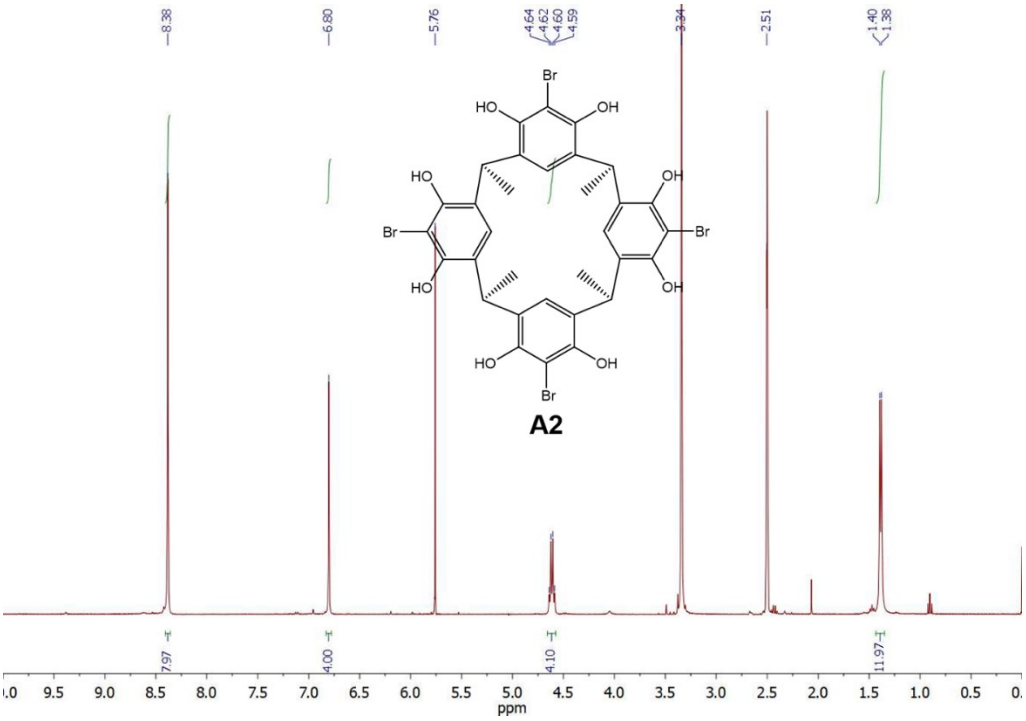

Figure S2: ^{1}H NMR Spectrum (400 MHz, $(CD_3)_2SO$) of **A2**

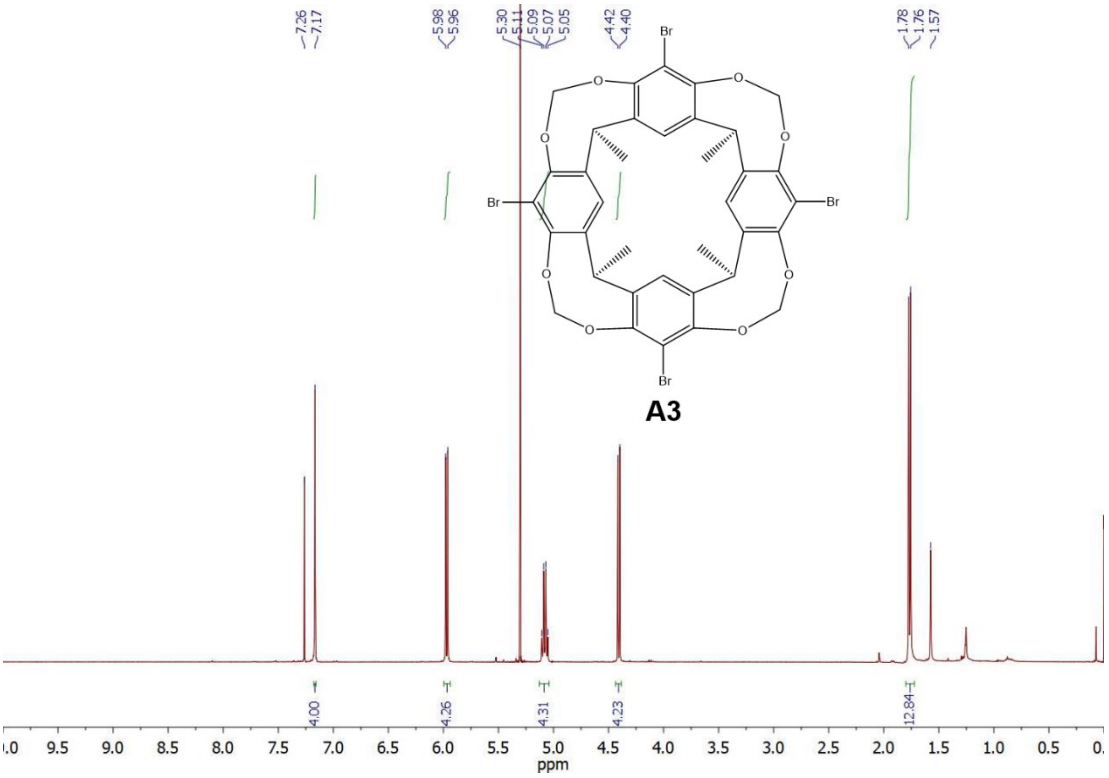

Figure S3: ^{1}H NMR Spectrum (400 MHz, $CDCl_3$) of **A3**

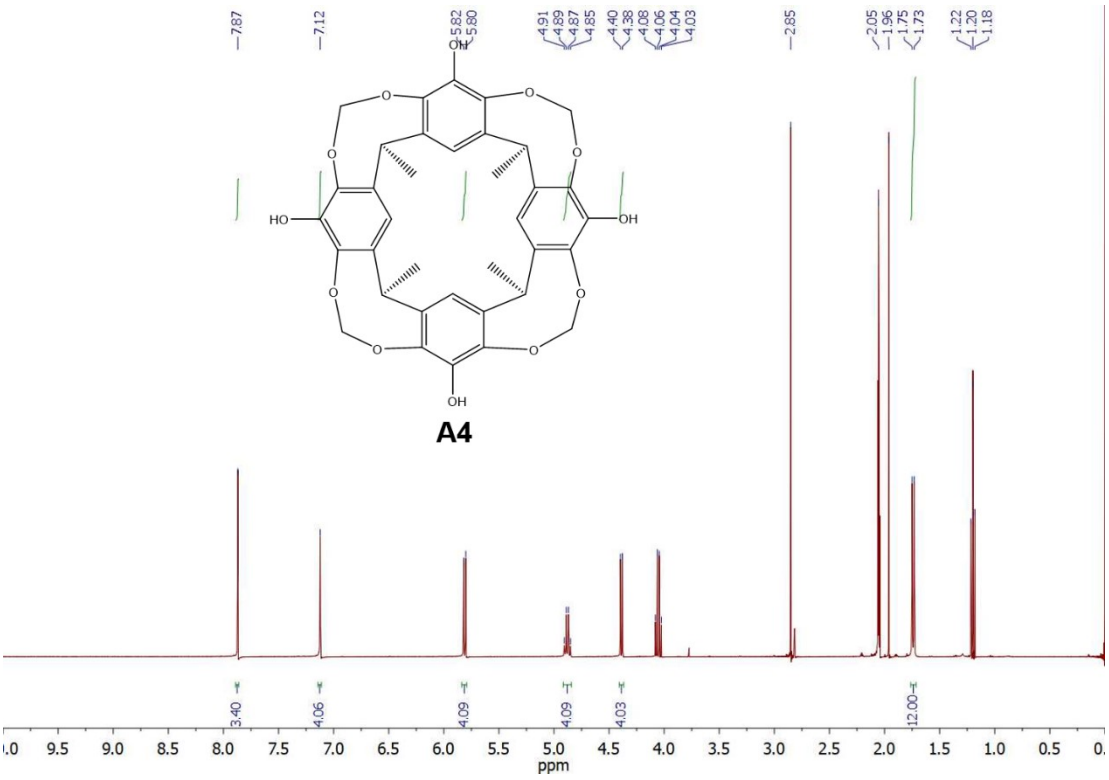

Figure S4: ^{1}H NMR Spectrum (400 MHz, $(CD_3)_2CO$) of **A4**

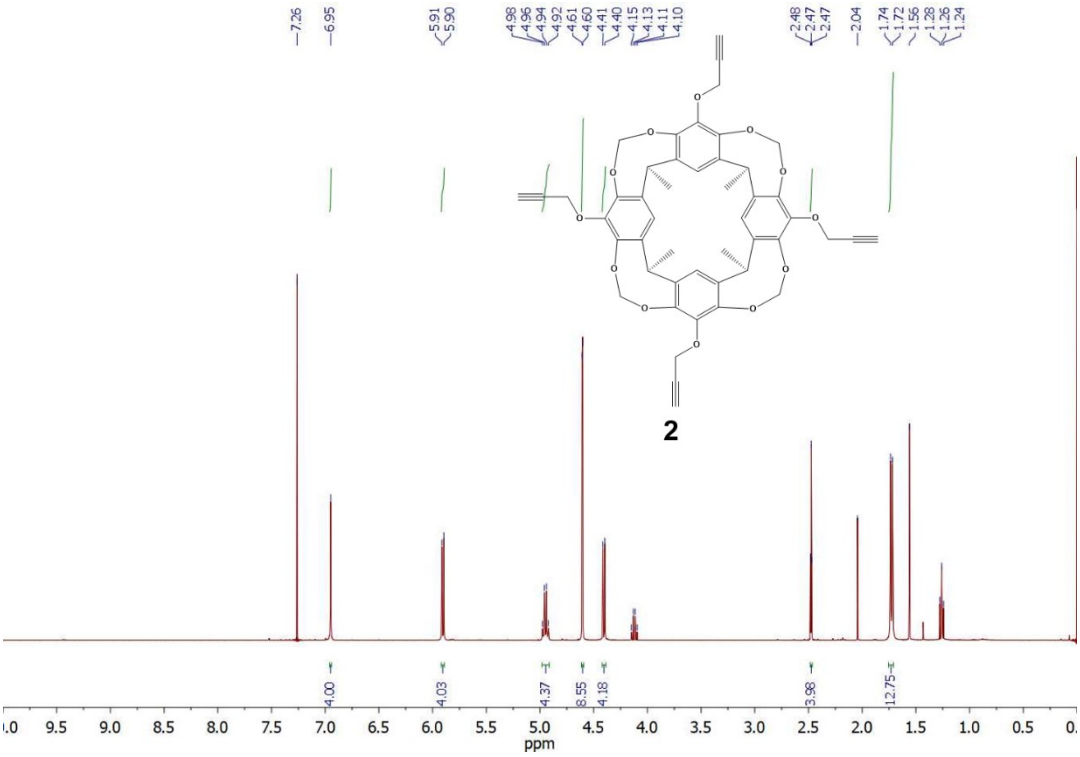

Figure S5: ^{1}H NMR Spectrum (400 MHz, $CDCl_3$) of **2**

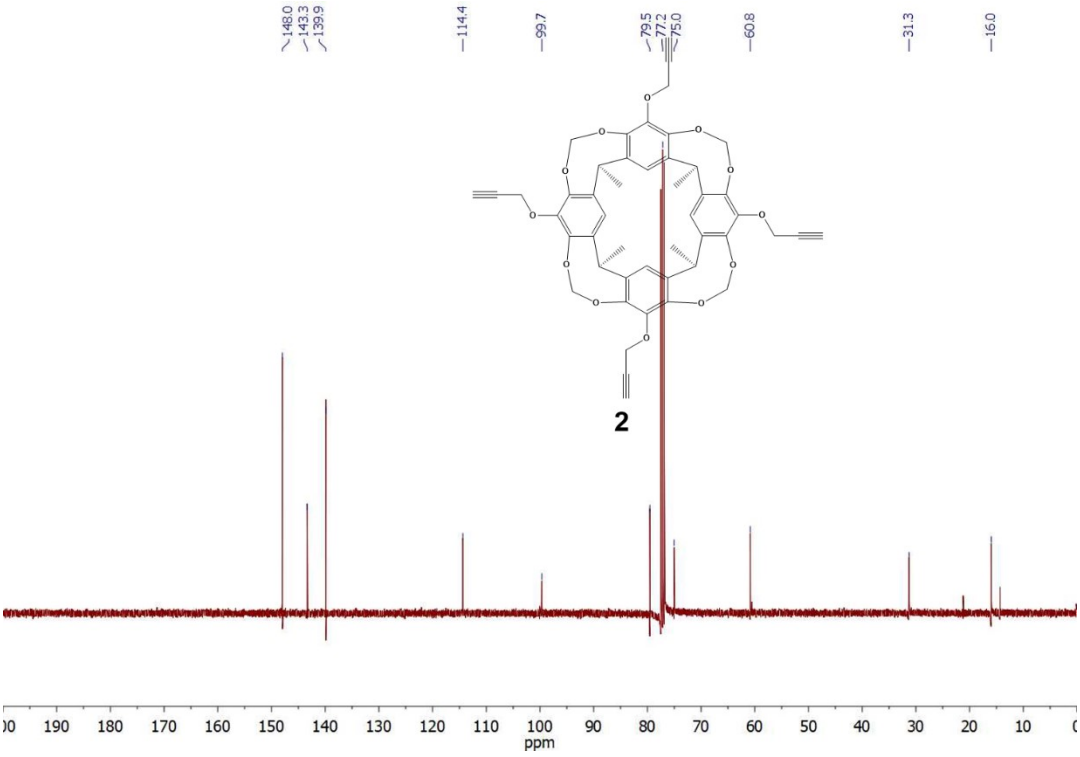

Figure S6: ^{13}C NMR Spectrum (100 MHz, $CDCl_3$) of **2**

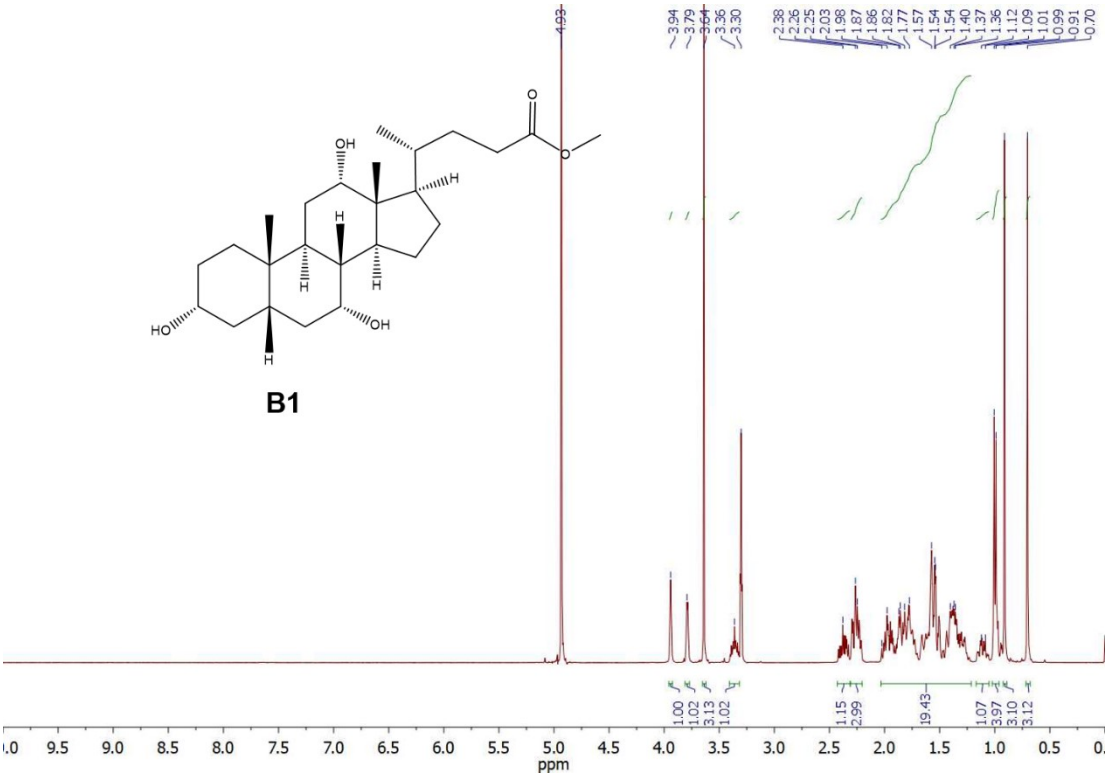

Figure S7: ^{1}H NMR Spectrum (400 MHz, CD_3OD) of **B1**

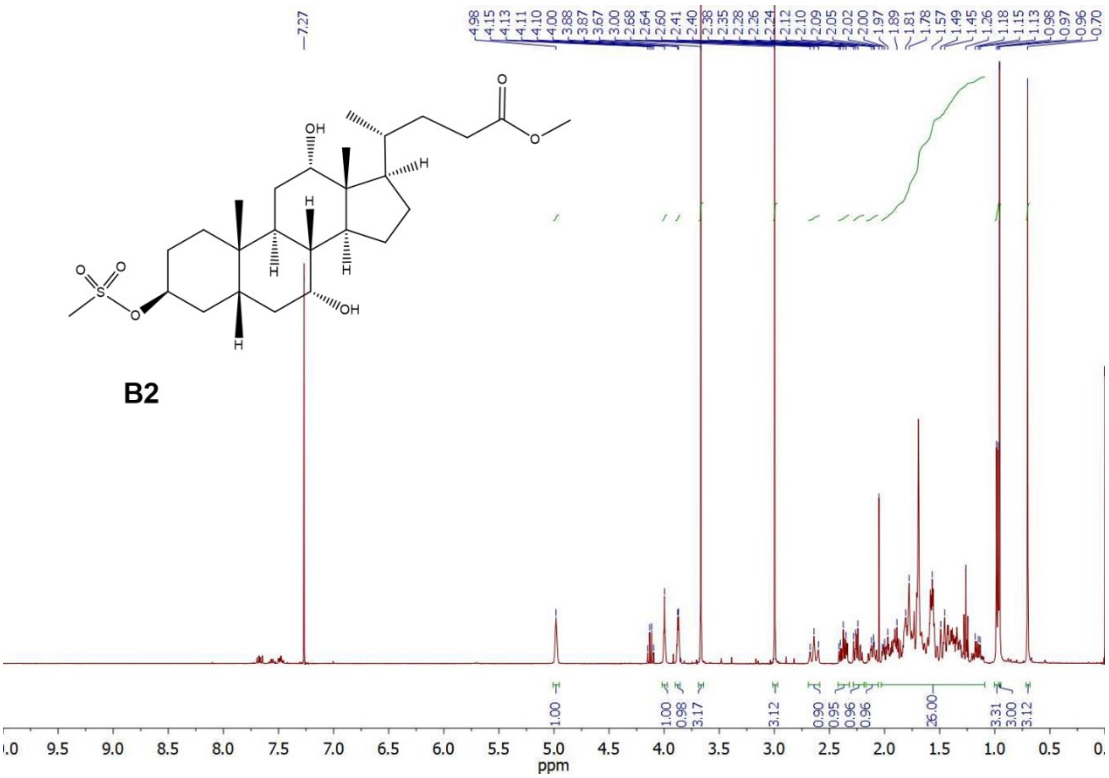

Figure S8: ^{1}H NMR Spectrum (400 MHz, $CDCl_3$) of **B2**

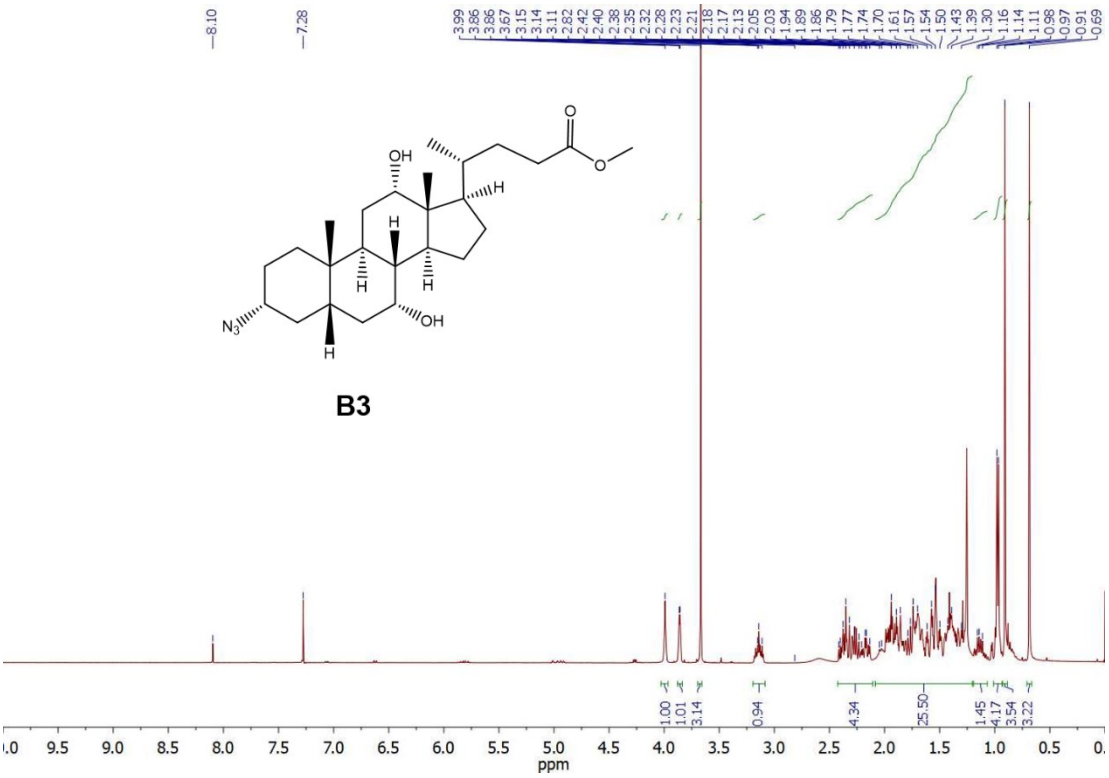

Figure S9: ^{1}H NMR Spectrum (400 MHz, $CDCl_3$) of **B3**

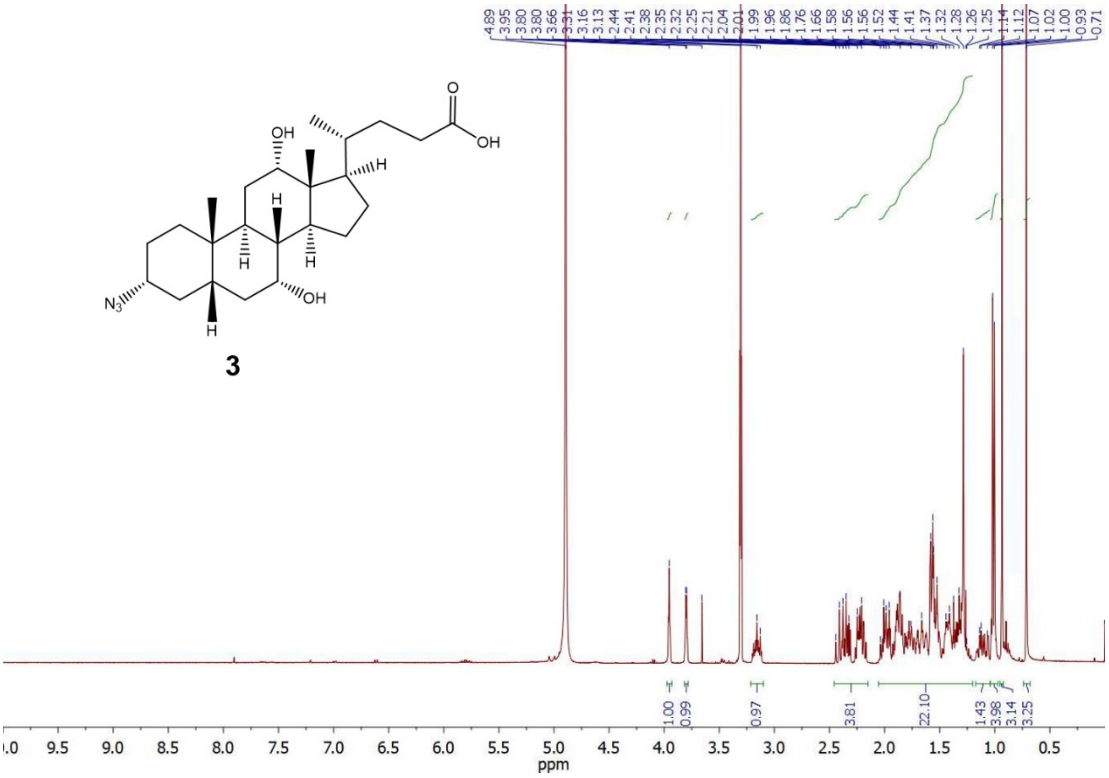

Figure S10: ^{1}H NMR Spectrum (400 MHz, CD_3OD) of **3**

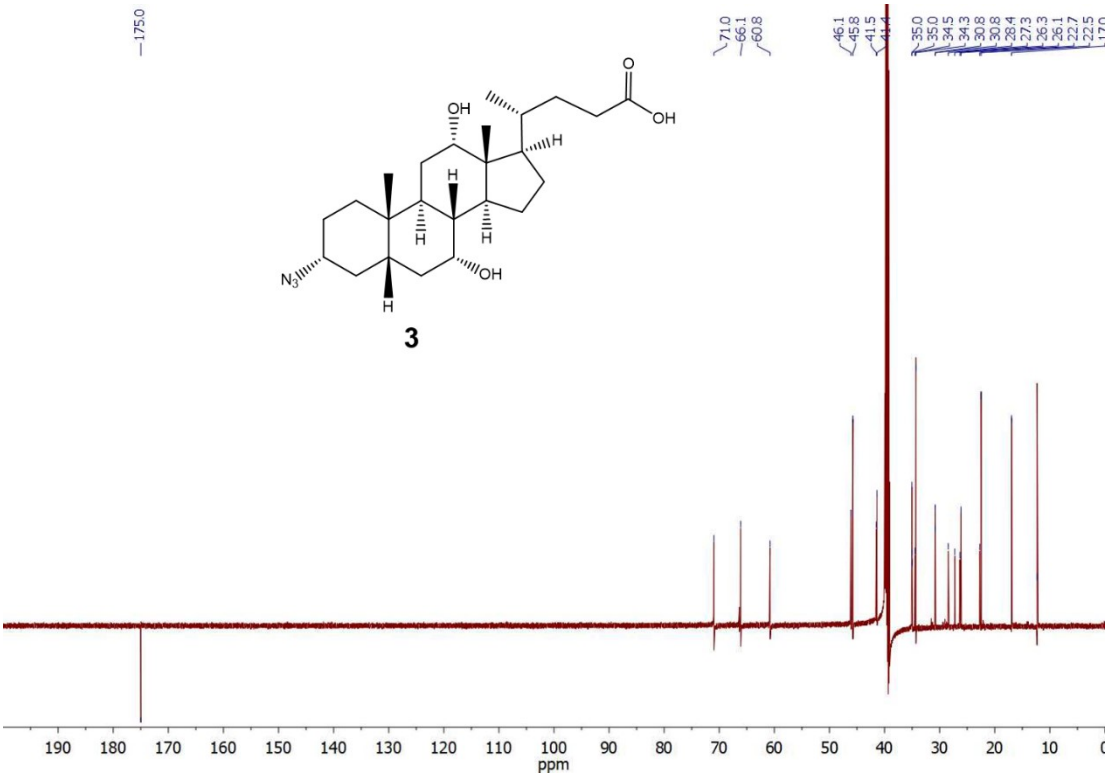

Figure S11: ^{13}C NMR Spectrum (100 MHz, $(CD_3)_2SO$) of **3**

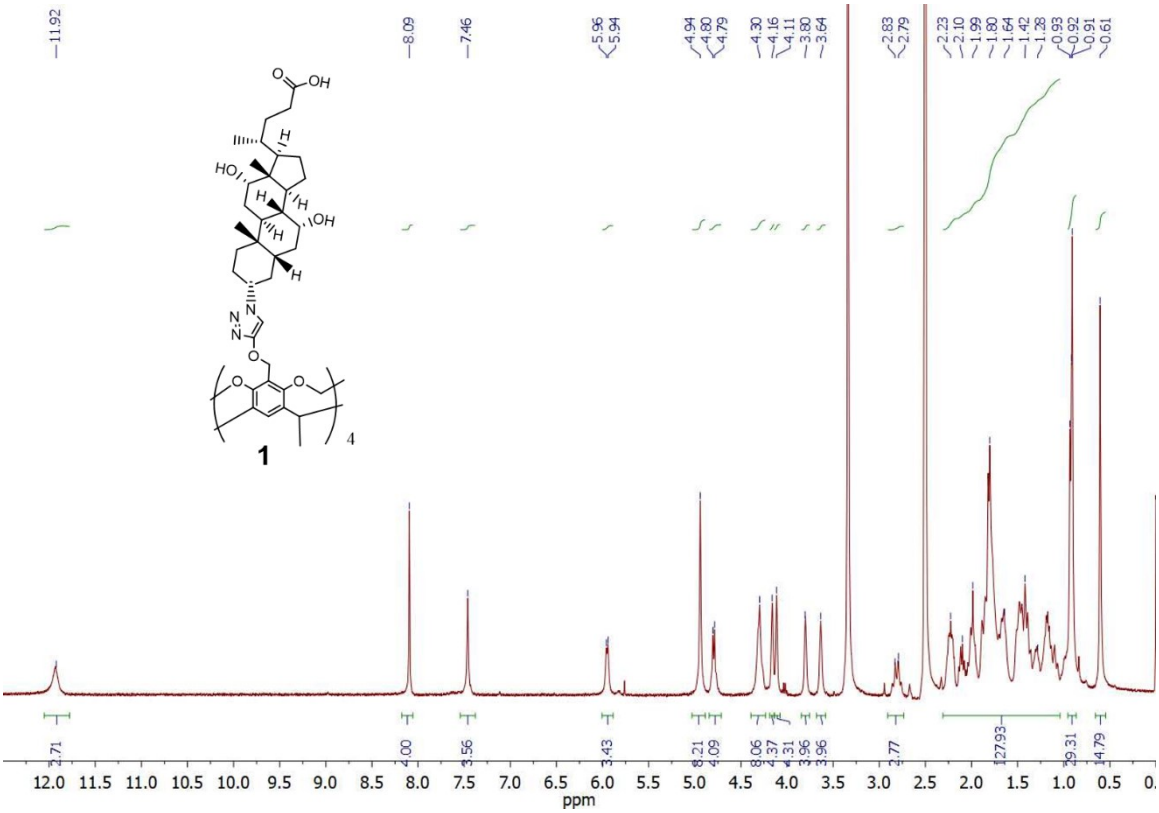

Figure S12: ^{1}H NMR Spectrum (400 MHz, $(CD_3)_2SO$) of **1**

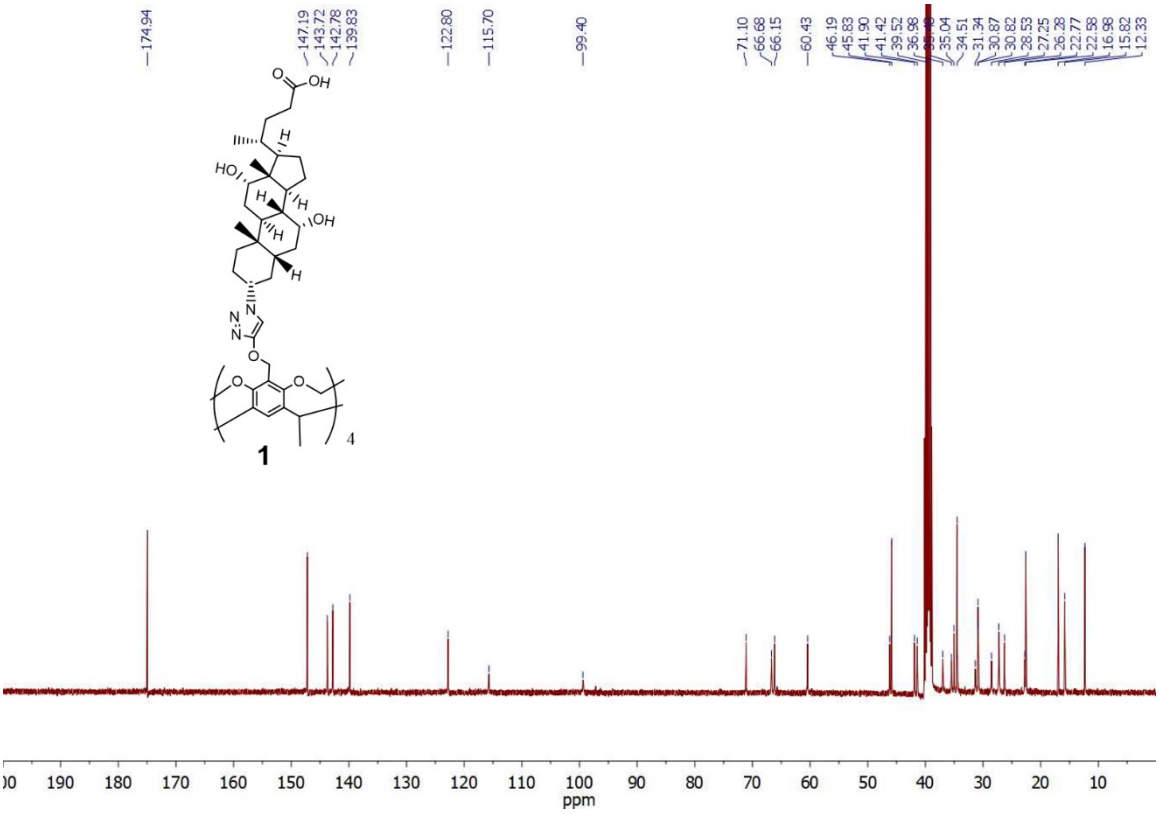

Figure S13: ^{13}C NMR Spectrum (100 MHz, $(CD_3)_2SO$) of **1**

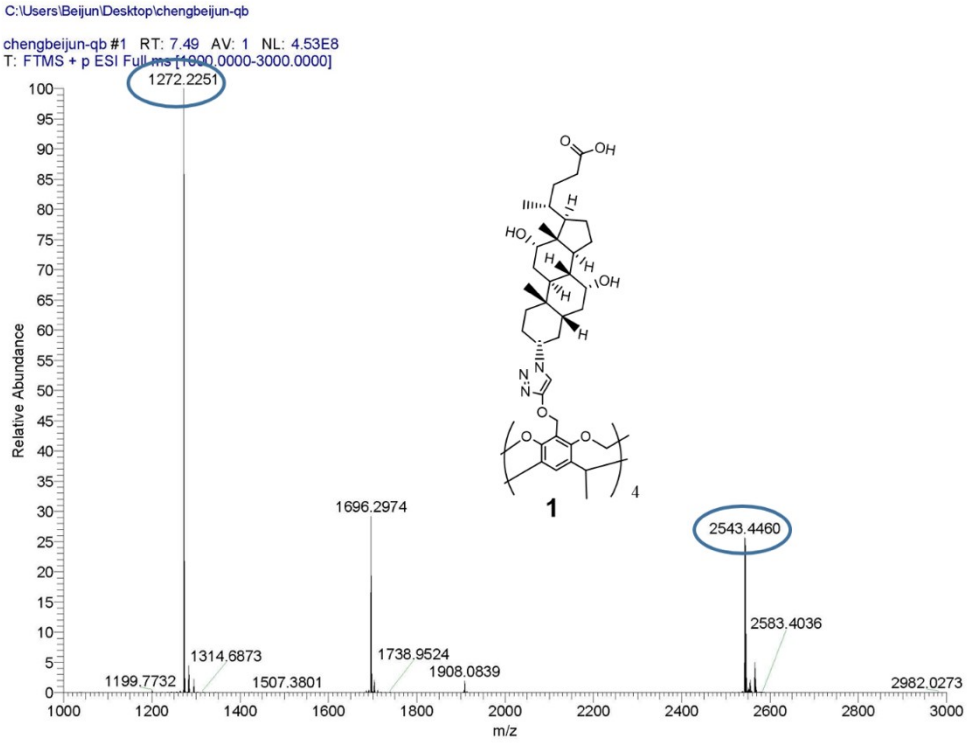

Figure S14: HRMS (ESI) *m/z*: (1) Found for $C_{144}H_{198}N_{12}O_{28}$ $[M + 2H]^{2+}$ 1272.2233; (2) Found for $C_{144}H_{197}N_{12}O_{28}$ $[M + H]^{+}$ 2543.4453

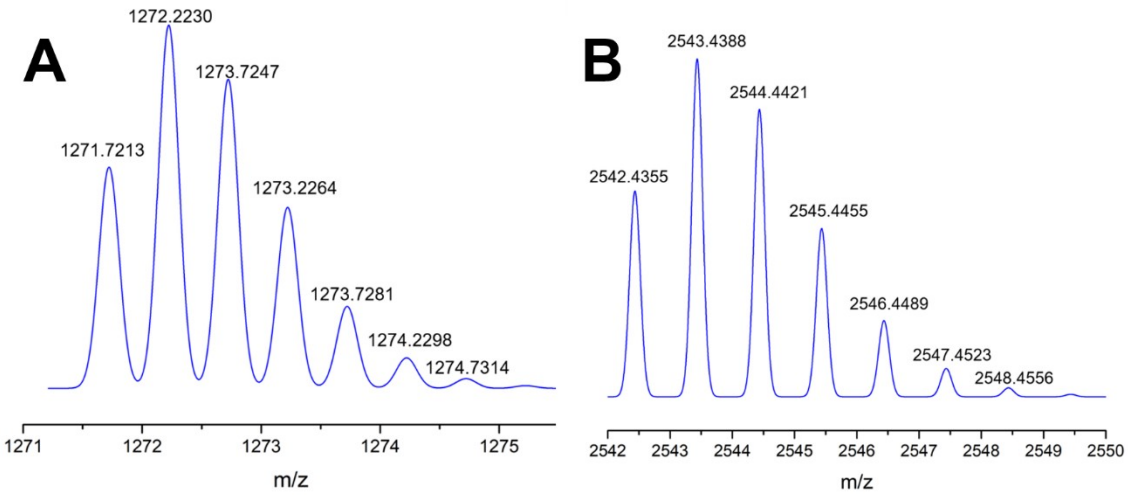

Figure S15: Simulated Isotopic Distribution for (A) $C_{144}H_{197}N_{12}O_{28}$ $[M + 2H]^{2+}$, and (B) $C_{144}H_{198}N_{12}O_{28}$ $[M + H]^{+}$.

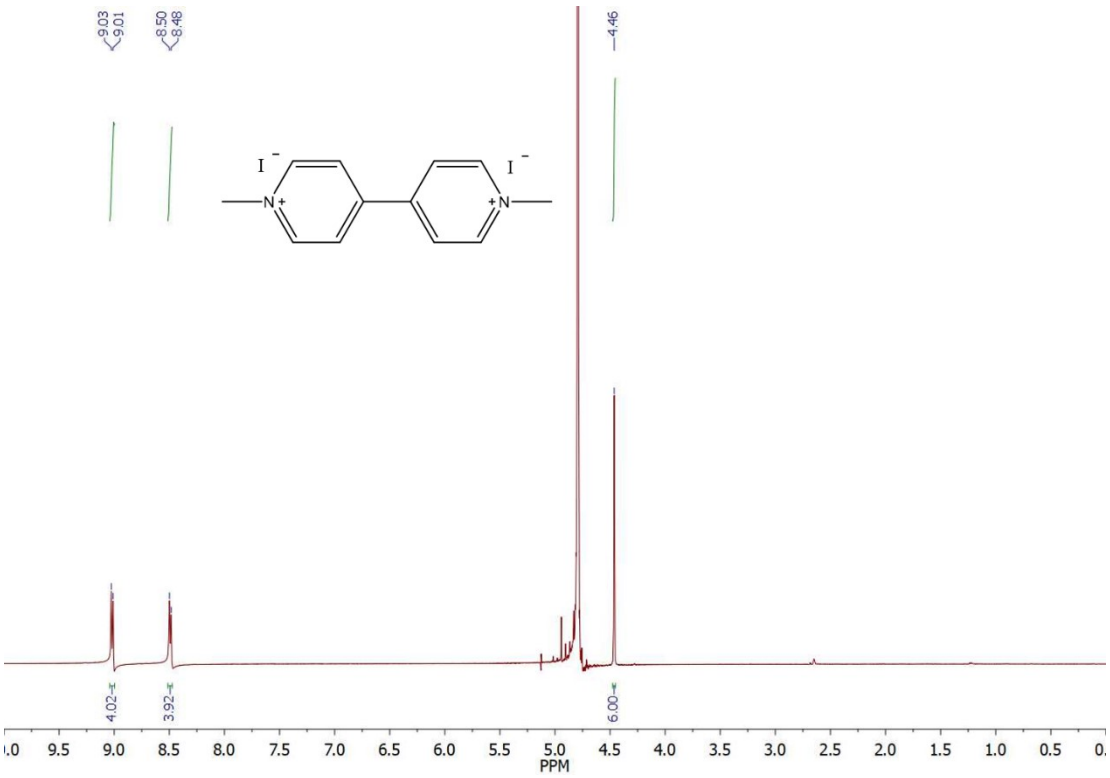

Figure S16: ^{1}H NMR Spectrum (400 MHz, D_2O) of **MV^{2+}**

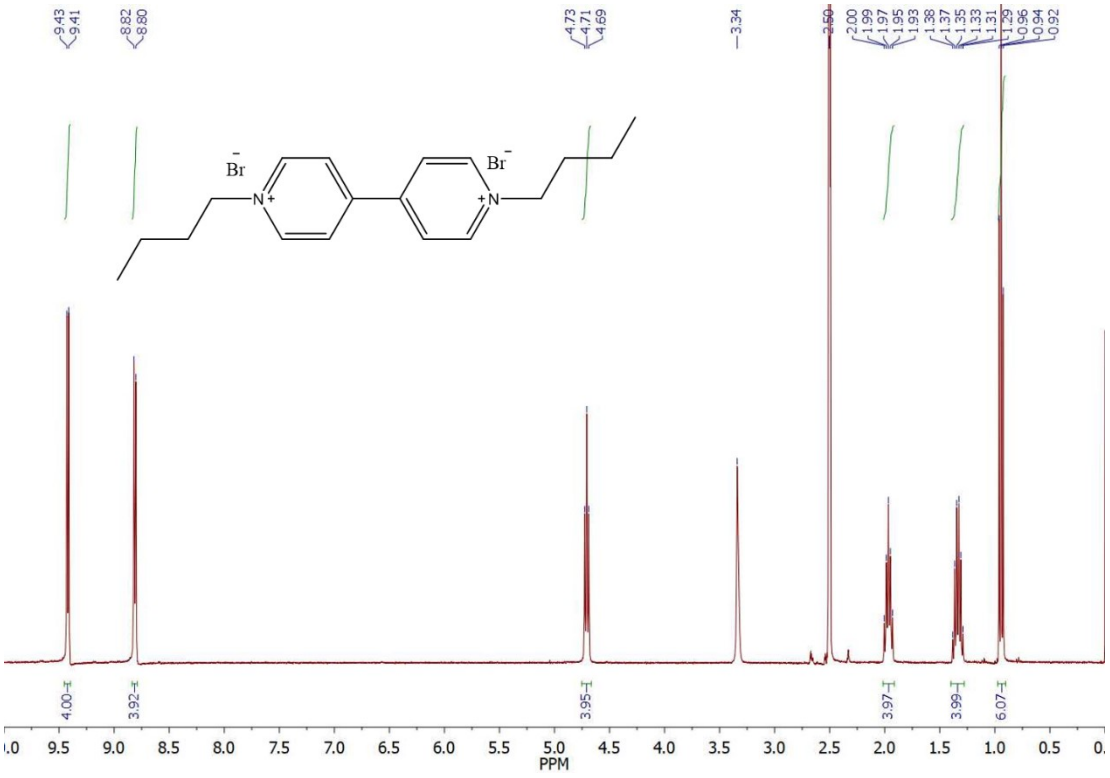

Figure S17: ^{1}H NMR Spectrum (400 MHz, $(CD_3)_2SO$) of **BV^{2+}**

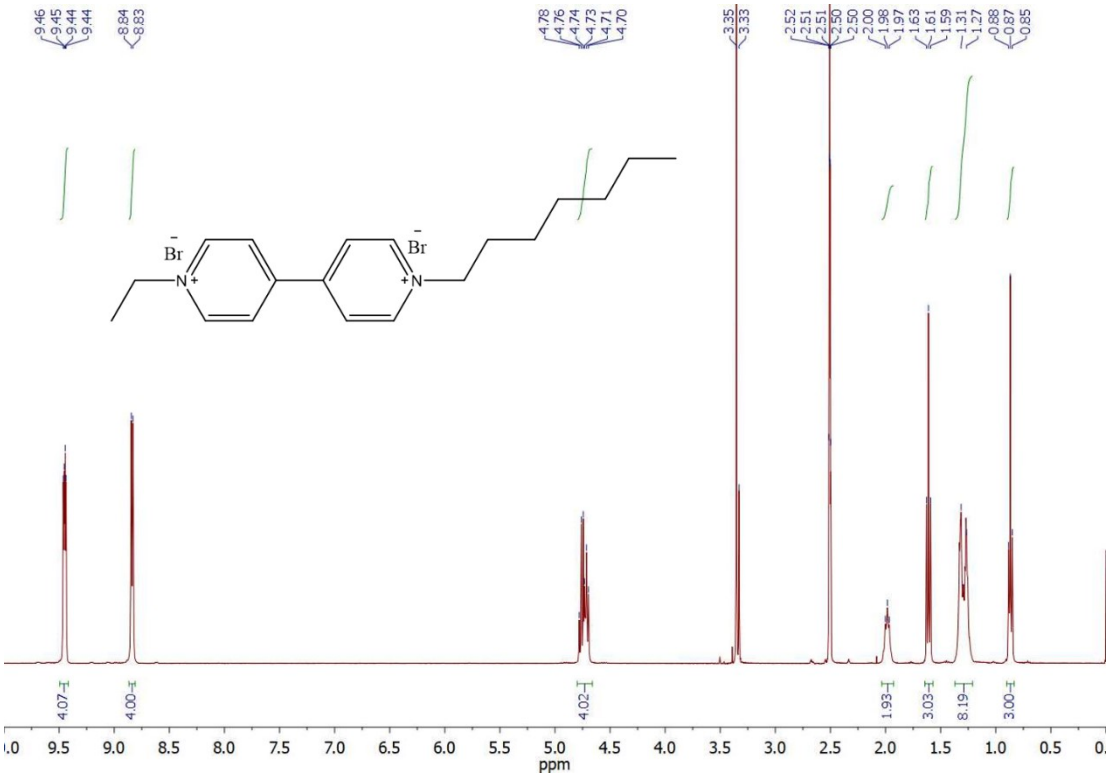

Figure S18: ^{1}H NMR Spectrum (400 MHz, $(CD_3)_2SO$) of **EHV^{2+}**

3. UV-vis Spectroscopy Studies

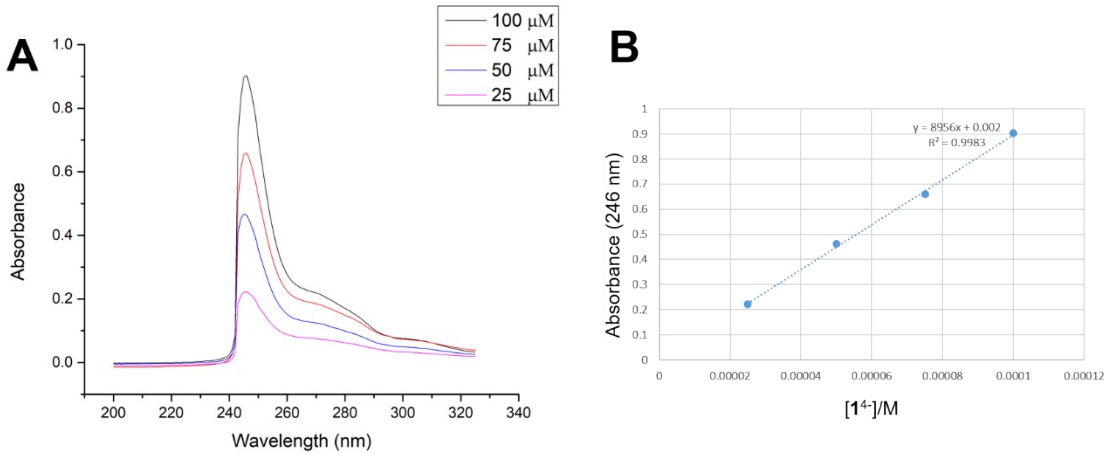

Figure S19: (A) UV-vis spectra of $\mathbf{1}^{4-}$ from 25 μM to 100 μM. (B) Linear relationship between absorbance at 246 nm and concentration of $\mathbf{1}^{4-}$ where ε=8956 $M^{-1}cm^{-1}$. Solvent: H_2O:DMSO (5:2, v/v, containing 40 mM sodium borate).

4. SWV data

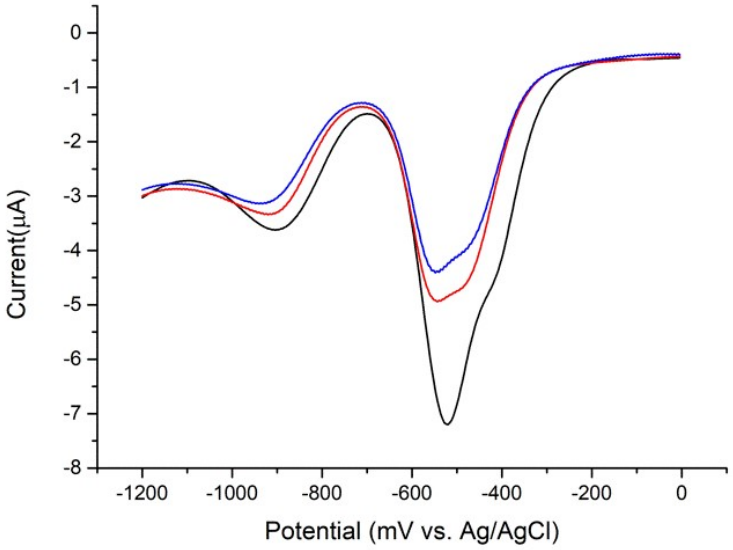

Figure S20: SWV responses of butyl viologen (0.1 mM) in H_2O-DMSO (5:2, v/v) on a glassy carbon electrode (0.071 cm^2) in the absence (black), in the presence of 1.0 equiv (red) and 2.0 equiv (blue) of tetracholine cavitand. Supporting electrolyte: sodium tetraborate (40 mM). The electrode potential was scanned from 0 mV to -1200 mV at 80 mV s^{-1}. Temperature: 25 °C.

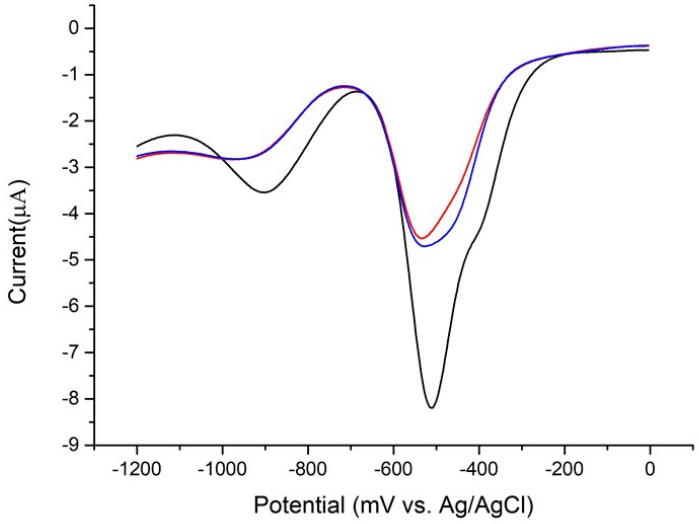

Figure S21: SWV responses of ethyl heptyl viologen (0.1 mM) in H_2O-DMSO (5:2, v/v) on a glassy carbon electrode (0.071 cm^2) in the absence (black), in the presence of 1.0 equiv (red) and 2.0 equiv (blue) of tetracholine cavitand. Supporting electrolyte: sodium tetraborate (40 mM). The electrode potential was scanned from 0 mV to -1200 mV at 80 mV s^{-1}. Temperature: 25 °C.

5. ESI-MS Spectra of $[1\bullet MV^{2+}]^{2+}$ and $[1\bullet BV^{2+}]^{2+}$

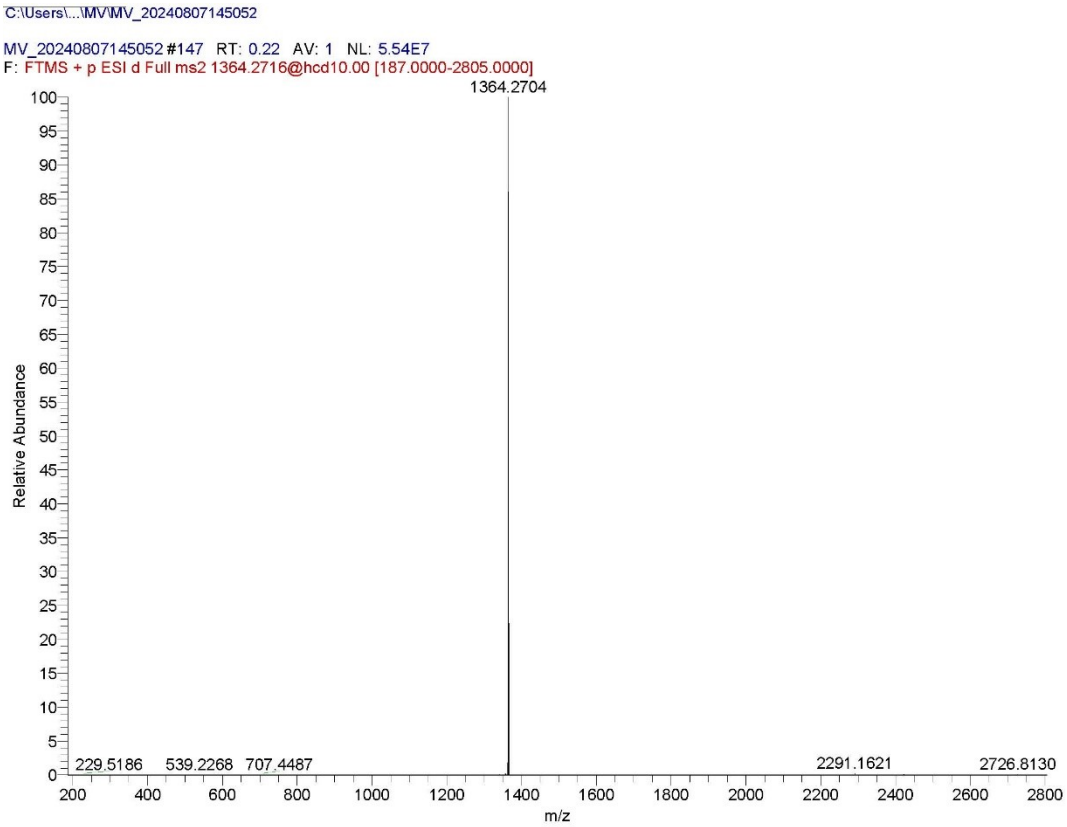

Figure S22: ESI-MS spectrum of $[\mathbf{1}\bullet MV^{2+}]^{2+}$

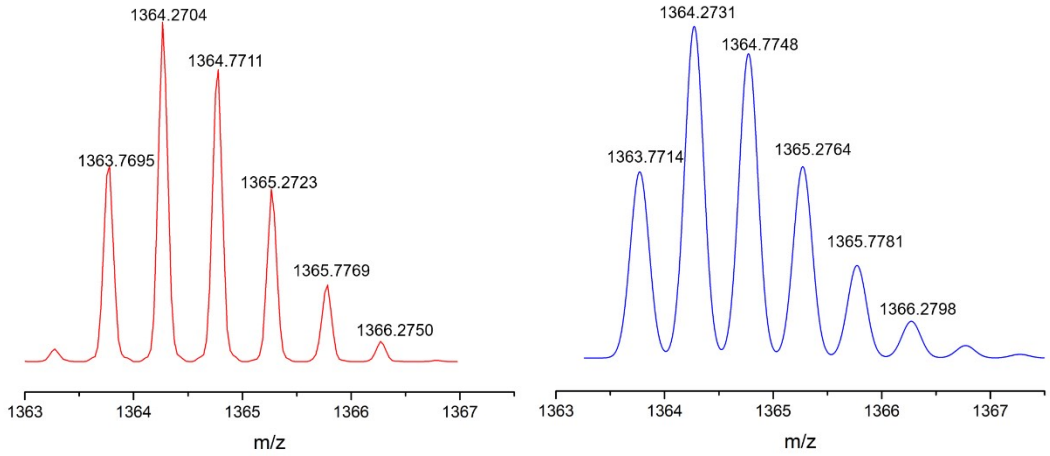

Figure S23: (Red) Experimental Isotopic Distribution of [**1**●MV^{2+}]$^{2+}$; (Blue) Simulated Isotopic Distribution of [**1**●MV^{2+}]$^{2+}$

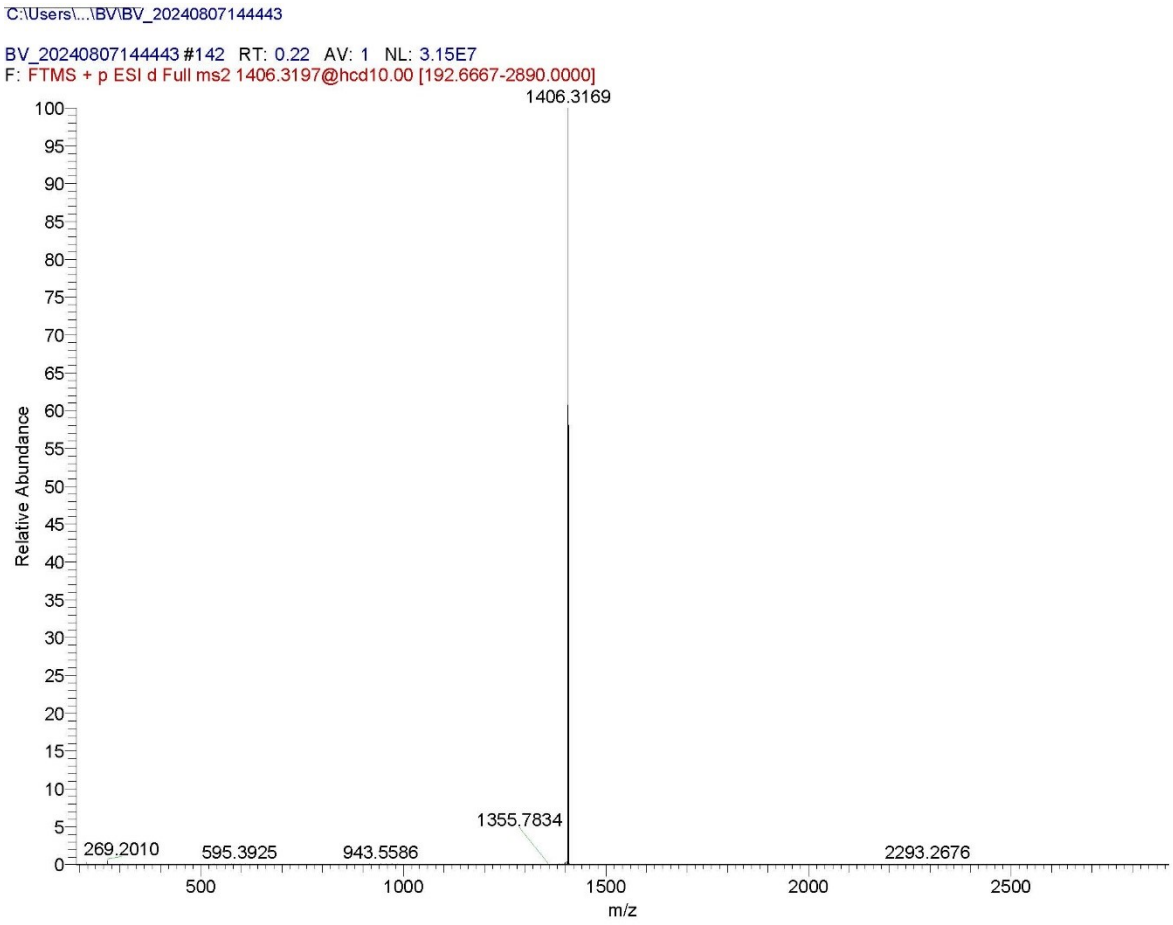

Figure S24: ESI-MS spectrum of [**1**●BV^{2+}]$^{2+}$

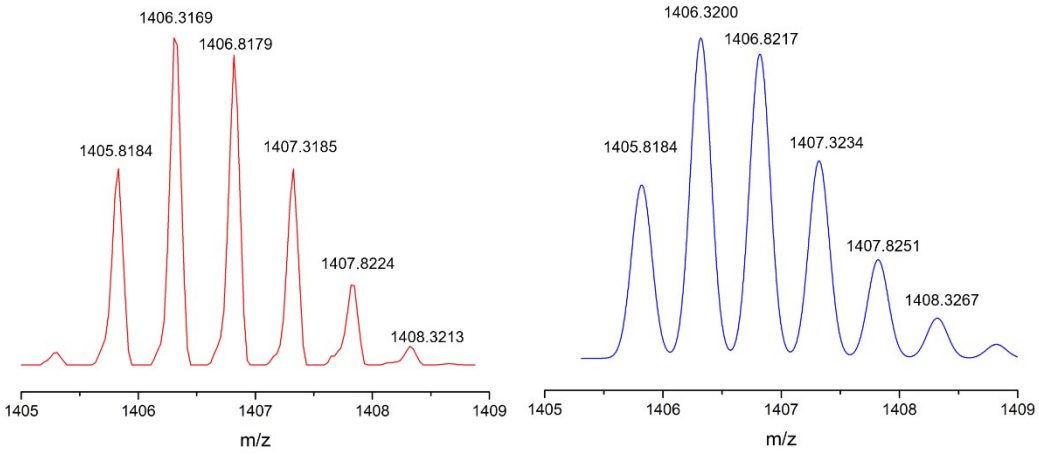

Figure S25: (Red) Experimental Isotopic Distribution of [**1**●BV^{2+}]$^{2+}$. (Blue) Simulated Isotopic Distribution of [**1**●BV^{2+}]$^{2+}$.

6. Computational details

All calculations reported herein were performed using the free-available program packages ORCA 5.0.3,[10] CREST 2.11.2,[11] and xTB 6.6.0.[12] Unless otherwise indicated, computations were carried out with default settings.

Initial geometries for the different species were generated by hand using the AVOGADRO software[13] and further optimized by using the GFF-xTB force field as implemented in xTB,[14] and including solvation effects in water by means of the analytical linearized Poisson-Boltzmann (ALPB) model.

Subsequent conformational searches for molecular species were carried out using the Conformer–Rotamer Ensemble Sampling Tool (CREST) with standard settings at the GFF-xTB/ALPB(water) level. The resulting conformational ensembles were re-optimized at the semiempirical GFN2-xTB tight binding method,[15] including solvation effects by means of the ALPB(water) model.[16] The lowest lying structures obtained in each case were corroborated as minima on the corresponding potential energy surface, by means of frequency calculations at the GFN2-xTB/ALPB(water) level using the software ORCA.

In the case of the host-guest complexes, representative binding modes were obtained by applying the recently reported aISS docking protocol developed by Grimme *et al* and implemented in xTB,[17] at the GFN2-xTB/ALPB(water) level of theory, starting in each case from the representative structures discussed above for host and guest obtained from the corresponding conformational searches. The best binding pose obtained in each case was subsequently corroborated as minima by frequency calculations.

Free energies of association ΔG_a° in aqueous solution for the H + G ⇌ G·H processes were calculated at the semiempirical (SQM) level following the supramolecular approach: $\Delta G_a^\circ = G^\circ_{aq}G{\subset}H - G^\circ_{aq}G - G^\circ_{aq}H$, where for each species X the free energy in aqueous solution was computed as $G^\circ(X) = [E_{gas}^{SQM}(X) + \delta_{solv}(X)] + G_{gas,mrrho}^\circ(X)$. Electronic $E_{aq}^{SQM}(X)$, and solvation energies $\delta_{solv}(X)$s, were evaluated concurrently using the GFN2-xTB/ALPB(water) scheme. Energy to free energy thermoestatical contributions $G_{gas,mrrho}^\circ$ were calculated by a modified rigid

rotor harmonic oscillator model, and derived from frequency calculations at the GFN2-xTB/ALPB(water) level. The concentration-induced free-energy shift of +1.89 kcal mol^{-1} was introduced for each reacting species, as required from the change of the estimated values of free energies in gas phase at 1 atm to 1 mol L^{-1} in solution.

Conformational analysis 1^{4-}

Truncated analogues of cavitand 1^{4-}

In order to keep the conformational analysis of cavitand $\mathbf{1}^{4-}$ on a computational budget, we devised the workflow shown in Scheme S10.

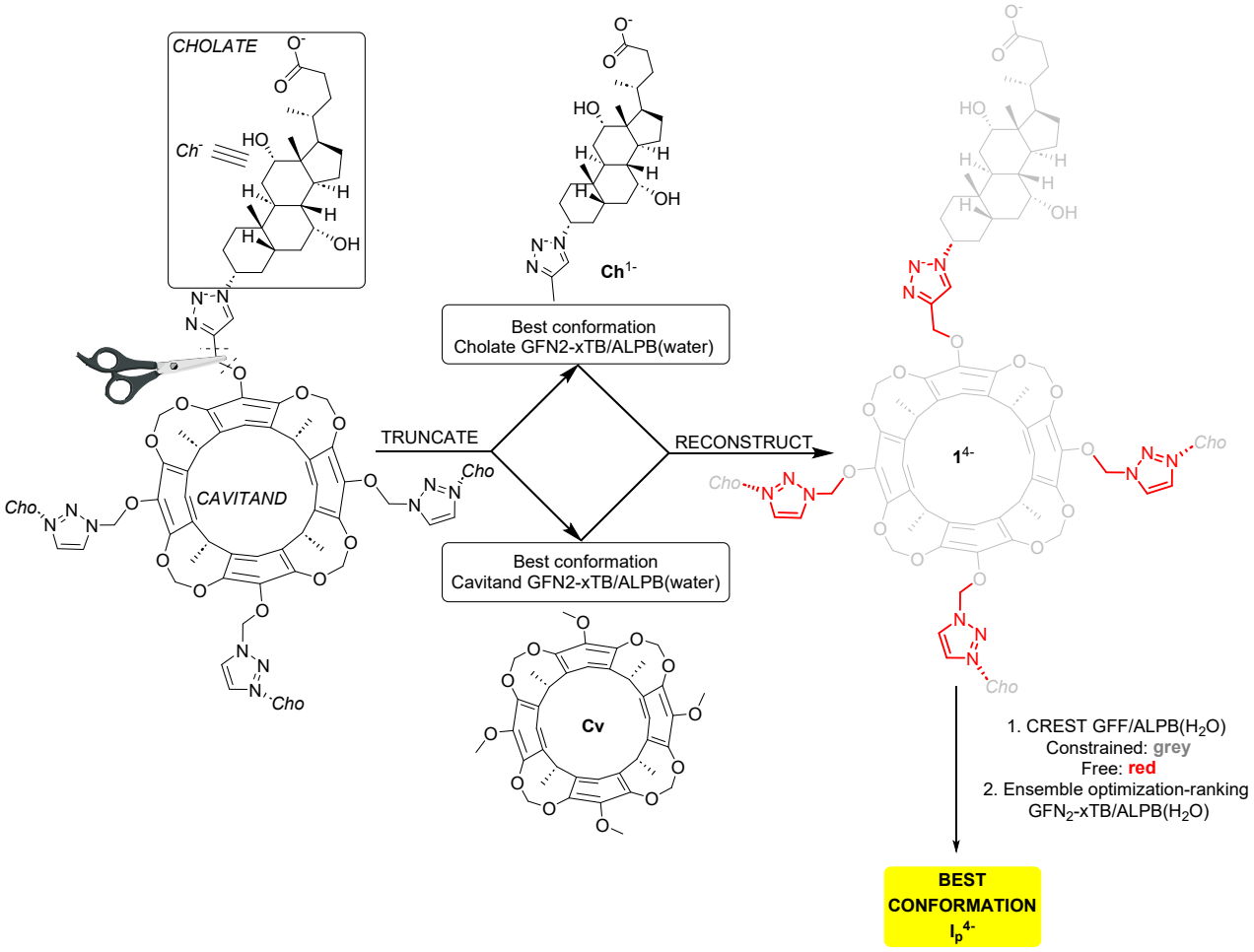

Scheme S10: Strategy followed for the simplified conformational analysis of $\mathbf{1}^{4-}$

As shown, we firstly analyzed the preferred conformations of the truncated analogues Cv and Cho^{1-} corresponding to the cavitand core and cholate moieties, respectively. From those, an initial biased geometry ($\mathbf{1}_i^{4-}$) was created by joining

the CV and Cho^- on their preferred conformations (structures Cv_p and Ch_p^-). Afterwards, a constrained conformational search was performed in order to establish the relative disposition of the four cholate substituents regarding the cavitand core. To that end, the conformational sampling on $\mathbf{1}_i^{4-}$ at the GFF-xtB/ALPB(water) level was executed, including only the atoms on the four triazolyl-based linker on the metadynamics-based sampling conducted by CREST. The obtained conformational ensemble was then further optimized and ranked at the GFN2-xTB/ALPB(water) level without constrains yielding the lowest lying conformer $\mathbf{1}_i^{4-}$. Finally, the obtained representative structures Cv_p, Ch_p^- and $\mathbf{1}_i^{4-}$ were all confirmed as true minima on the potential energy surface of the corresponding species by frequency analysis.

Regarding the truncated cavitand Cv, as shown in Figure S26, the conformational sampling produced as a result only one preferred minima for the species Cv_p, reproducing the expected C_4 symmetry of the macrocyle.[1]

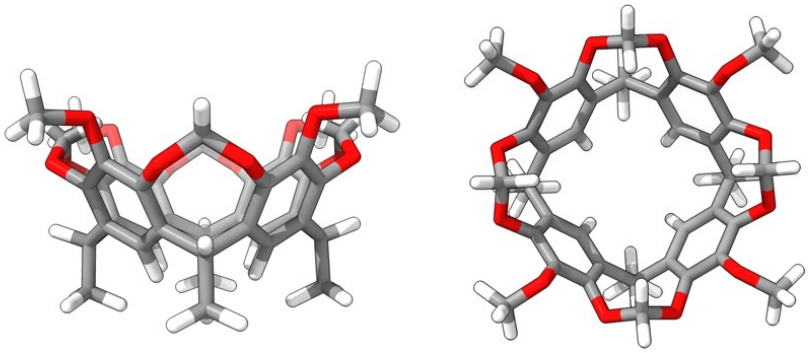

Figure S26: Side and top views of the structure Cv_p of the minima found for the truncated cavitand Cv at the GFN2-xTB/ALPB(water) level. C: dark grey, O: red, H: off-white

In the case of the cholate moiety, accounting for its higher degrees of freedom, the conformational sampling with CREST resulted in 104 unique structures at the GFN2-XTB/ALPB(water) level. Nonetheless, those share the same expected axial disposition of the triazole moiety, being the conformational variance restricted to the carboxylate-containing chain. The structure of the lowest-lying conformer is shown in Figure S27.

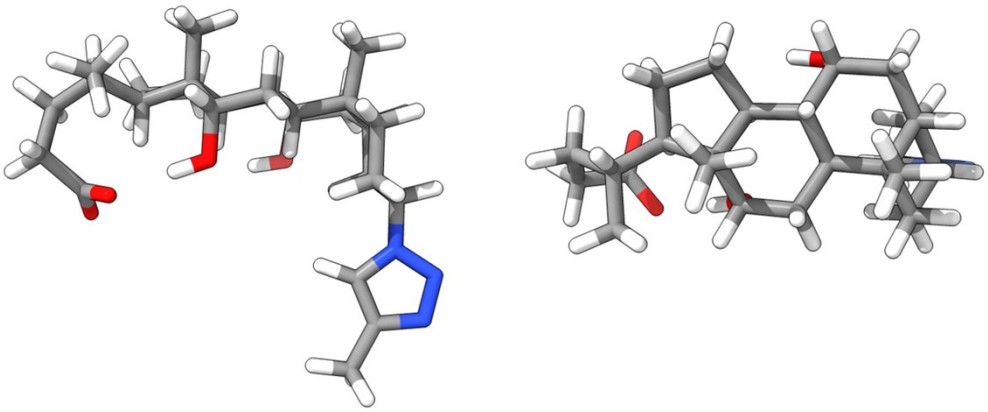

Figure S27: Side and top views of a stick representation of the structure Ch_p^- of the minima found for the truncated cholate moiety Ch^- GFN2-xTB/ALPB(water) level. C: dark grey, N: blue, O: red, H: off-white.

Biased conformational analysis of cavitand 1^{4-}

With the preferred conformations of the cavitand and cholate subunits in our hands, we proceeded to perform the constrained conformational analysis of the complete species $\mathbf{1}^{4-}$. As shown in Figure S28, the obtained preferred conformation $\mathbf{1_p}^{4-}$ for the species shows a globular structure with two of the cholate subunits blocking the upper cavity of the cavitand core, and the other two wrapped around the macrocycle. This conformation can be explained on the basis of the inability of the cholate units to dispose their hydrophilic hydroxyl-containing faces to the aqueous environment, an orientation that comes imposed by the union of those with the macrocycle trough the α-C3 atom. As so, the compact structure would try to maximize the solvation of the highly hydrophobic species by decreasing as much as possible the solvent-accessible surface area.

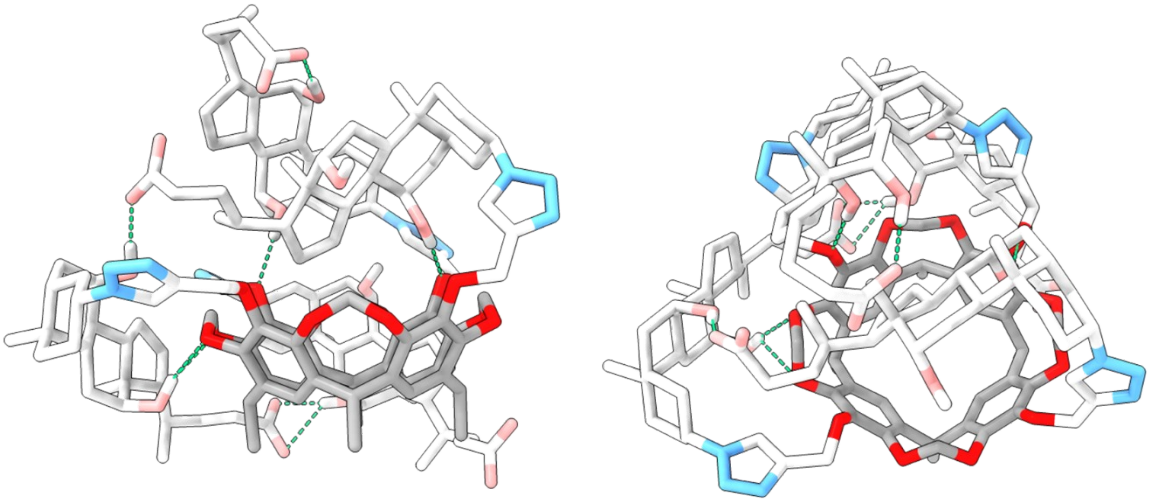

Figure S28: Side and top views of a stick representation the structure of the minima 1_p^{4-} found for the preferred conformation of 1^{4-} at the GFN2-xTB/ALPB(water) level of theory. For clarity, non-polar hydrogens atoms are omitted, C: dark grey (cavitand) and light grey (cholate), N: light blue, O: red (cavitand) and light red (cholate). Intramolecular hydrogen bonds shown as dashed green lines.

In addition to $\mathbf{1_p^{4-}}$, the preferred obtained conformation for the tetracholate-cavitand hybrid, we explored a biased alternative conformation of the species that would expand the cavity of the macrocycle by an appropriate arrangement of the cholate substituents. That was initially constructed by hand, by imposing to the triazolyl-containing linkers a perpendicular disposition regarding the cavitand core, and the cholate subunits arranged as far as possible from the cavity of the macrocycle core. Optimization of this structure at the GFN2-xTB/ALPB(water) level produced a minimum on the potential energy surface of the species, $\mathbf{1_b^{4-}}$, which structure is depicted in Figure S29. As shown, this idealized geometry dispose the 4 cholate arms on C2 rotation axis, with the hydrophilic face of the substituents directed to the cavitand core, and generating a cavity of 335 $Å^3$.[18] Comparison of the free energies for both $\mathbf{1_p^{4-}}$ and $\mathbf{1_b^{4-}}$ results on a difference of 18.6 kcal/mol in favor of the globular compact structure.

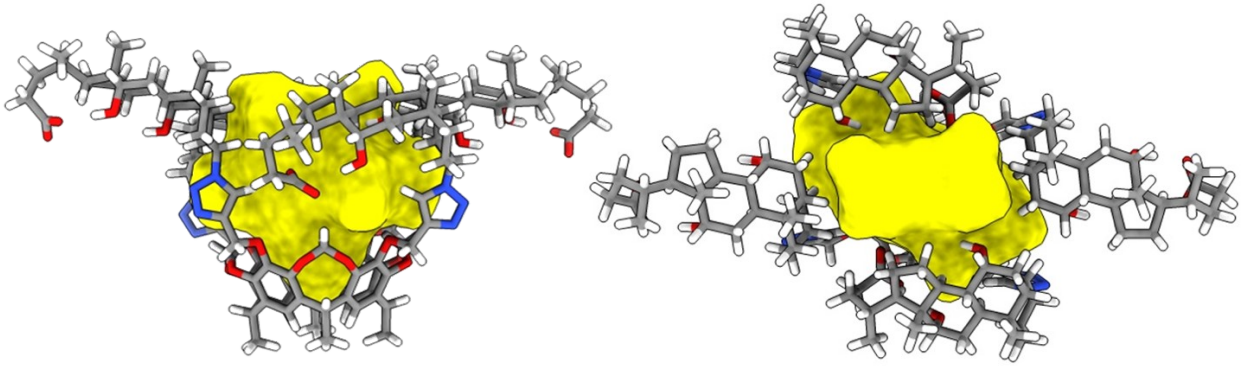

Figure S29: Side and top views of a stick representation the structure of the minima 1_p^{4-} with the cavity volume represented as a yellow surface. C: dark grey, N: blue, O: red, H: off-white.

Host-guest docking study

In order to evaluate the interaction of $\mathbf{1}^{4-}$ with methyl viologen (MV^{2+}) as guest we employed the recently-developed automated computational interaction site screening (aISS) workflow, which makes use of a genetic algorithmic search supported by the intermolecular force-field xTB-IFF, followed by application of the GFN2-xTB/alpb(water) for the geometry optimization of the obtained solutions (by default 15), and their subsequent ranking on the basis of electronic energies as the final step. This procedure was applied to both $\mathbf{1}_p^{4-}$ and $\mathbf{1}_b^{4-}$ as starting geometries of the cholate-cavitand hybrid.

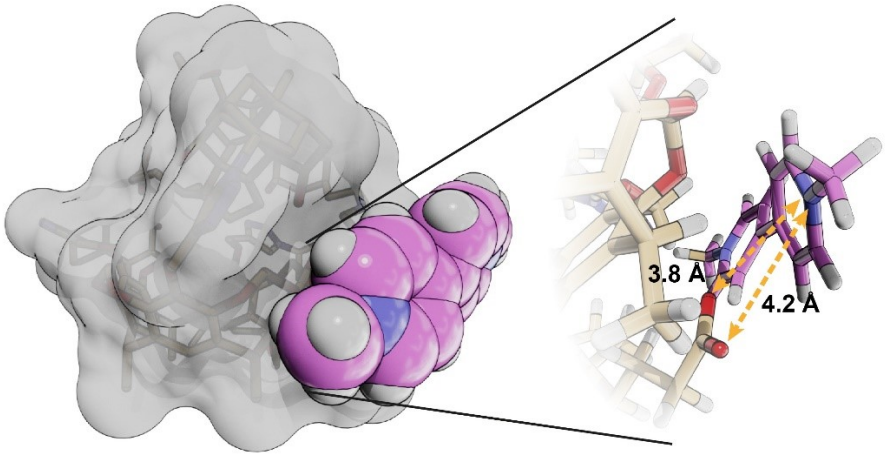

Figure S30: Energy-minimized structure for the most favored complex formed by cavitand 1_p^{4-} (van der Waals surface) and guest MV^{2+} (van de Waals spheres, C: violet, N: blue, H: white) found using the aISS docking protocol. The magnified image on the right shows the spatial proximity between one of the carboxylate groups.

As shown in Figure S30, the best pose BP_a^{2-} obtained from the workflow consist on the placement of the MV^{2+} guest on a lateral of the cavitand core, with one of the carboxylate groups of the guest near enough to establish an electrostatic attraction with the cationic substrate without a significant distortion of the initial conformation of the host.

In the case of the idealized $\mathbf{1_b}^{4-}$ structure as initial conformation for the host, the docking workflow renders as the best pose BP_b^{2-} a geometry in which, although the MV^{2+} is partially inserted into the cavity generated within the host (Figure S31), its initial volume has been significantly reduced during the optimization process at the GFN2-xTB/alpb(water), accounting for the discussed tendency of the species to reduce its hydrophobic surface by adopting a more globular conformation.

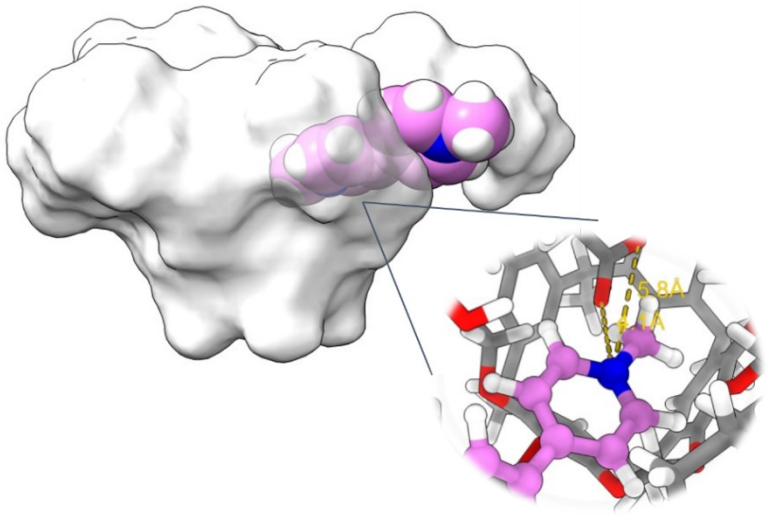

Figure S31: Energy-minimized structure for the most favored complex formed by cavitand 1_b^{4-} (van der Waals surface) and guest MV^{2+} (van de Waals spheres, C: violet, N: blue, H: white) found using the aISS docking protocol. The magnified image on the right shows the spatial proximity between one of the carboxylate groups.

Finally, the free energy of association $\Delta G_a°$ was computed at the GFN2-xTB/ALPB(water) level, using the preferred conformation $\mathbf{1_p}^{4-}$ as reference for the host. In both cases, the values obtained for the association reveal the association as clear exergonic processes, being $\Delta G_a°$ (BP_a^{2-}) = -10.00 kcal/mol and $\Delta G_a°$ (BP_b^{2-}) = -11.48 kcal/mol. Consequently, at this level of theory, it can be asserted that a potential exergonic interaction between host and guest can be established without the need of the generation of an inclusion complex.

7. References

(1) Cram, D. J.; Karbach, S.; Kim, H.-E.; Knobler, C. B.; Maverick, E. F.; Ericson, J. L.; Helgeson, R. C. Host-Guest Complexation. 46. Cavitands as Open Molecular Vessels Form Solvates. *J. Am. Chem. Soc.* 1988, **110,** 2229.

(2) Roman, E.; Peinador, C.; Mendoza, S.; Kaifer, A. E. Improved Synthesis of Cavitands. *J. Org. Chem.* 1999, **64,** 2577.

(3) Fraser, J. R.; Borecka, B.; Trotter, J.; Sherman, J. C. An Asymmetric Carceplex and New Crystal Structure Yield Information Regarding a 1 Million-Fold Template Effect. *J. Org. Chem.* 1995, **60,** 1207.

(4) Timmerman, P.; Nierop, K. G. A.; Brinks, E. A.; Verboom, W.; van Veggel, F. C. J. M.; van Hoorn, W. P.; Reinhoudt, D. N. Hydrophobic Concave Surfaces and Cavities by Combination of Calix[4]arenes and Resorcin[4]arenes. *Chem. Eur. J.* 1995, **1,** 132.

(5) Cram, D. J.; Jaeger, R.; Deshayes, K. Host-Guest Complexation. 65. Hemicarcerands that Encapsulate Hydrocarbons with Molecular Weights Greater than Two Hundred. *J. Am. Chem. Soc.* 1993, **115,** 10111.

(6) Dayal, B.; Speck, J.; Bagan, E.; Tint, G. S.; Salen, G. p-Toluenesulfonic Acid/Methanol: Mild Reagent for the Preparation of Bile Acid Methyl Esters. *Steroids* 1981, **37,** 239.

(7) Thota, B. N. S.; Savyasachi, A. J.; Lukashev, N.; Beletskaya, I. Maitra U. Tripodal Bile Acid Architectures Based on a Triarylphosphine Oxide Core Obtained by Copper-Catalysed [1,3]-Dipolar Cycloaddition: Synthesis and Preliminary Aggregation Studies. *Eur. J. Org. Chem.* 2014, **2014,** 1406.

(8) Zhao, Y.; Zhong, Z. Oligomeric Cholates: Amphiphilic Foldamers with Large Internal Hydrophobic Cavities. *J. Am. Chem. Soc.* 2005, **127,** 17894.

(9) Massarenti, C.; Bortolini, O.; Fantin, G.; Cristofaro, D.; Ragno, D.; Perrone, D.; Marchesi, E.; Toniolo, G.; Massi, A. Fluorous-tag Assisted Synthesis of Bile Acid-bisphosphonate Conjugates *via* Orthogonal Click Reactions: an Access to Potential Anti-resorption Bone Drugs. *Org. Biomol. Chem.* 2017, **15,** 4907.

(10) Neese, F. Software update: The ORCA program system—Version 5.0. *WIREs Comput Mol Sci*. 2022, **12,** e1606.

(11) Pracht, P.; Bohle, F.; Grimme, S.; Automated exploration of the low-energy chemical space with fast quantum chemical methods. *Phys. Chem. Chem. Phys.*, 2020**, 22,** 7169.

(12) Bannwarth, C.; Caldeweyher, E.; Ehlert, S.; Hansen, A.; Pracht, P.; Seibert, J.; Spicher, S.; Grimme, S. Extended tight-binding quantum chemistry methods. *WIREs Comput. Mol. Sci.* 2021, **11,** e1493

(13) Hanwell, M. D.; Curtis, D. E.; Lonie, D. C.; Vandermeersch, T.; Zurek, E.; Hutchison, G. R. Avogadro: An advanced semantic chemical editor, visualization, and analysis platform. *J. Cheminform.* 2012, **4,** 17.

(14) Spicher, S.; Grimme, S.; Robust atomistic modeling of materials, organometallic and biochemical system. *Angew. Chem. Int. Ed.* 2020**, 59,** 15665.

(15) Ehlert, S.; Stahn, M.; Spicher, S.; Grimme, S. Robust and Efficient Implicit Solvation Model for Fast Semiempirical Methods. *J. Chem. Theory Comput.* 2021, **17,** 4250.
(16) Bannwarth, C.; Ehlert, S.; Grimme S. GFN2-xTB—An Accurate and Broadly Parametrized Self-Consistent Tight-Binding Quantum Chemical Method with Multipole Electrostatics and Density-Dependent Dispersion Contributions. *J. Chem. Theory Comput.* 2019, **15,** 1652.
(17) Plett, C.; Grimme, S. Automated and Efficient Generation of General Molecular Aggregate Structures, *Angew. Chem. Int. Ed.* 2023, **62,** e202214477.
(18) Martí-Centelles, V.; Piskorz, T. K.; Duarte, F. CageCavityCalc (C3): A computational tool for calculating and visualizing cavities in Molecular Cages. *ChemRxiv*, 2024, https://doi.org/10.26434/chemrxiv-2024-fmlx0.